Models for α-Keto Acid-Dependent Non-heme Iron Enzymes: Structures and Reactivity of [Fe^{II}(L)(O$_2$CCOPh)](ClO$_4$) Complexes[†]

Yu-Min Chiou and Lawrence Que, Jr.*

*Contribution from the Department of Chemistry, University of Minnesota, Minneapolis, Minnesota 55455*

Received November 16, 1994[⊕]

Abstract: The first iron(II)−α-ketocarboxylate complexes were synthesized with the use of tetradentate tripodal ligands tris[(6-methyl-2-pyridyl)methyl]amine (6TLA) and tris(2-pyridylmethyl)amine (TPA) and benzoylformate (BF) as the α-keto acid to model the putative iron−cofactor interaction in the active site of α-keto acid-dependent non-heme iron enzymes. [Fe^{II}(6TLA)(BF)](ClO$_4$) (**1**) crystallizes in the triclinic system, space group $P\bar{1}$ (no. 2) with cell constants $a = 8.931(6)$ Å, $b = 13.366(7)$ Å, $c = 15.160(7)$ Å, $\alpha = 75.92(4)°$, $\beta = 81.06(5)°$, $\gamma = 70.78(5)°$, $V = 1652(4)$ Å^3, and $Z = 2$; $R = 0.071$ and $R_w = 0.082$. [Fe^{II}(TPA)(BF)(MeOH)](ClO$_4$)·2MeOH (**2**·MeOH) crystallizes in the orthorhombic system, space group $Pca2_1$ (no. 29) with cell constants $a = 19.875(6)$ Å, $b = 8.916(4)$ Å, $c = 18.02(1)$ Å, $V = 3193(4)$ Å^3, and $Z = 4$; $R = 0.054$ and $R_w = 0.056$. The BF ligand chelates to the iron in **1** via one carboxylate oxygen and the carbonyl oxygen, but binds to the iron in **2** only through a carboxylate oxygen, with a methanol solvate occupying the other site. Both complexes react with dioxygen and quantitatively convert to decarboxylated complexes [Fe^{II}(6TLA)(OBz)]$^+$ (**5**) and [Fe$^{III}_2$O(TPA)$_2$(OBz)$_2$]$^{2+}$ (**6**), respectively. Both **1** and **2** react with substrates 2,4-di-*tert*-butylphenol and triphenylphosphine under an O$_2$ atmosphere to afford the corresponding biphenol and OPPh$_3$, respectively. ^{18}O$_2$-labeling experiments show incorporation of one ^{18}O atom into the respective benzoate products and one into the OPPh$_3$. Kinetic studies on a series of [Fe^{II}(6TLA)(X-BF)](ClO$_4$) complexes show pseudo-first-order disappearance of their characteristic color in the presence of excess dioxygen. The rate of the oxidative decarboxylation is sensitive to the nature of the phenyl substituent, exhibiting a Hammett ϱ value of +1.07 which indicates a nucleophilic mechanism. A reaction mechanism is proposed consisting of dioxygen binding to the iron(II) center, forming an iron(III)−superoxide species, attack of the nascent superoxide on the BF keto carbon, oxidative decarboxylation affording the oxidizing species, and substrate oxidation. Complexes **1** and **2** represent the first structural and functional models for α-keto acid-dependent non-heme iron enzymes.

Introduction

α-Keto acid-dependent non-heme iron enzymes[1−3] function in diverse metabolic processes, including the post-translational hydroxylation of proline and lysine residues in vertebrate collagen[4] and the biosynthesis of microbial cephalosporins.[5,6] Despite their diverse functions, these enzymes all require the combination of a mononuclear Fe(II) center, an α-keto acid, and O$_2$ to effect 2e$^-$ oxidation of substrates concomitant with the oxidative decarboxylation of the keto acid. For hydroxy-lases, the elements of molecular oxygen are incorporated into the hydroxyl group of the product and the carboxylate derived from the oxidation of the keto function of the keto acid cofactor (eq 1).

$$\text{S} + O_2 + \text{RCOCOOH} \rightarrow \text{S}O + \text{RCO}O\text{H} + \text{CO}_2 \quad (1)$$
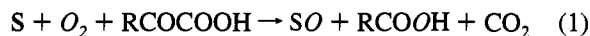
Because of the dependence on an α-keto acid cofactor, these enzymes may have a common reaction mechanism, and one has been proposed on the basis of the available data on prolyl 4-hydroxylase.[2] This mechanism consists of (a) dioxygen binding to the iron(II) center to form an iron(III)−superoxide species, (b) attack of this superoxide on the keto carbon of the iron-bound α-keto acid, (c) decarboxylation of the α-keto acid to generate the oxidizing species, (d) hydroxylation of the substrate, and (e) product release.

The nonenzymatic decarboxylation of α-keto acids is difficult to accomplish, since the carbonyl group in an α-keto acid is in a position where it cannot delocalize the negative charge that results from decarboxylation.[7,8] Therefore, an electron acceptor is required in the oxidative decarboxylation process. Indeed a number of oxidants are known to cause rapid, quantitative decarboxylation of α-keto acids,[9] including Fe(II)/H$_2$O$_2$.[10]

---

(1) Abbott, M. T.; Udenfriend, S. In *Molecular Mechanisms of Oxygen Activation*; Hayaishi, O., Ed.; Academic Press: New York, 1974; pp 167−214.

(2) Hanauske-Abel, H. M.; Günzler, V. *J. Theor. Biol.* **1982**, *94*, 421−455.

(3) Kivirikko, K. I.; Myllylä, R.; Pihlajaniemi, T. *FASEB J.* **1989**, *3*, 1609−1617.

(4) Kivirikko, K. I.; Myllylä, R.; Pihlajaniemi, T. In *Post-Translational Modifications of Proteins*; Harding, J. J., Crabbe, M. J. C., Eds.; CRC Press: Boca Raton, FL, 1992; pp 1−51.
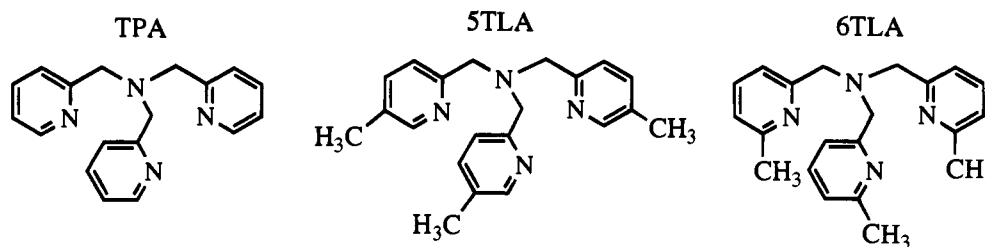
(5) Baldwin, J. E.; Adlington, R. M.; Crouch, N. P.; Schofield, C. J.; Turner, N. J.; Aplin, R. T. *Tetrahedron* **1991**, *47*, 9881−9900.

(6) Townsend, C. A.; Basak, A. *Tetrahedron* **1991**, *47*, 2591−2602.

(7) Hanson, R. W. *J. Chem. Educ.* **1987**, *64*, 591−595.

(8) Walsh, C. *Enzymatic Reaction Mechanisms*; Freeman: San Francisco, 1979; pp 682−683.

Chart 1. Tripodal Ligands

TPA   5TLA   6TLA

However, there are no nonenzymatic examples of oxidative decarboxylation of α-keto acids utilizing dioxygen as oxidant and no well-characterized iron complexes of α-keto acids. Thus, to investigate the chemical role of the iron in biological oxidations catalyzed by α-keto acid-dependent enzymes and to develop an understanding of the reaction mechanism, we have initiated the synthesis and mechanistic study of the first Fe-(II)−α-keto acid model complexes. We report herein the structures and reactivities of the ternary complexes [Fe^{II}(L)-(BF)]$^+$, where L is one of the tripodal tetradentate ligands shown in Chart 1 and BF is benzoylformate. Comparisons of their spectroscopic and kinetic properties afford insights into the nature of the putative iron−cofactor interaction in the proposed enzymatic reactions. Some of our results have been previously communicated.[11]

Experimental Section

General Materials and Procedures. All reagents and solvents were purchased from commercial sources and used as received unless noted otherwise. Triphenylphosphine (Aldrich) was recrystallized from EtOH prior to use and checked by ^{31}P NMR for purity. CH_3CN was distilled from CaH_2 prior to use. Labeled dioxygen ($^{18}O_2$; 99.2 atom % ^{18}O) and water ($H_2{}^{18}O$; 96.7 atom % ^{18}O) were obtained from Isotec, Inc. Preparations and handling of air-sensitive materials were carried out under an argon atmosphere using standard Schlenk techniques or in a Vacuum Atmospheres TS-5000 anaerobic box. Deoxygenation of solvents and solutions was effected by repeated vacuum/purge cycles using argon. Elemental analyses were performed by M-H-W Laboratories, Phoenix, AZ.

Ligands. 6TLA[12] and TPA·3HClO$_4$[13] were synthesized according to published procedures. Benzoylformic acid and its sodium salt were purchased from Aldrich. (*m*-Nitrobenzoyl)formic acid was prepared by nitration of benzoylformic acid with concentrated HNO_3/H_2SO_4 in 70% yield: ^{1}H NMR (acetone-d_6) δ 7.9 (t, 1H), 8.5 (d, 1H), 8.6 (d, 1H), 8.9 (s, 1H), 12.3 (br s, 1H); ^{13}C NMR (acetone-d_6) δ 125, 129, 131, 134, 136, 149, 164 (COOH), 185 (CO); EI-MS *m/z* (relative intensity) 195 (M$^+$, 7), 178 (M$^+$ − OH, 20), 150 (M$^+$ − COOH, 100). The ethyl esters of (*p*-chlorobenzoyl)formic acid, (*p*-fluorobenzoyl)-formic acid, (*p*-methylbenzoyl)formic acid, and (*p*-methoxybenzoyl)-formic acid were prepared by treating ethyl α-oxo-1*H*-imidazole-1-acetate with the appropriate aryl Grignard reagent.[14] Phenyl-substituted benzoylformic acids were obtained in 75−90% yields by base-catalyzed hydrolysis of the resulting ethyl esters with 4 N NaOH$_{(aq)}$ at room temperature for 4 h. *p*-Cl-BF-H: ^{1}H NMR (CDCl$_3$) δ 7.5 (d, 2H), 8.3 (d, 2H), 9.2 (br s, 1H); ^{13}C NMR (CDCl$_3$) δ 129, 130, 133, 143, 161 (COOH), 183 (CO); EI-MS *m/z* (relative intensity) 184 (M$^+$, 2), 139 (M$^+$ − COOH, 100), 111 (M$^+$ − COCOOH, 32). *p*-F-BF-H: ^{1}H NMR (CDCl$_3$) δ 7.2 (m, 2H), 8.3 (m, 2H), 9.6 (br s, 1H); ^{13}C NMR (CDCl$_3$) δ 115, 128, 134, 163, 169 (COOH), 183 (CO); EI-MS *m/z* (relative intensity) 149 (M$^+$ − F, 8), 123 (M$^+$ − COOH, 100), 95 (M$^+$ −

COCOOH, 37). *p*-CH$_3$-BF-H: ^{1}H NMR (CDCl$_3$) δ 2.4 (s, 3H), 7.2 (d, 2H), 7.9 (br s, 1H), 8.1 (d, 2H); ^{13}C NMR (CDCl$_3$) δ 22 (CH$_3$), 129, 130, 131, 147, 164 (COOH), 185 (CO); EI-MS *m/z* (relative intensity) 119 (M$^+$ − COOH, 100), 91 (M$^+$ − COCOOH, 48). *p*-OCH$_3$-BF-H: ^{1}H NMR (acetone-d_6) δ 3.9 (s, 3H), 7.1 (d, 2H), 8.0 (d, 2H), 10.5 (br s, 1H); ^{13}C NMR (acetone-d_6) δ 55.5 (OCH$_3$), 114.6, 125.6, 132.5, 165.1, 165.4 (COOH), 185.9 (CO); EI-MS *m/z* (relative intensity) 180 (M$^+$, 7), 135 (M$^+$ − COOH, 100), 107 (M$^+$ − COCOOH, 12).

Complexes. [Fe^{II}(6TLA)(BF)](ClO$_4$) (1). A methanol solution of 6TLA (0.33 g, 1.0 mmol) and sodium benzoylformate (0.17 g, 1.0 mmol) was added to 1 equiv of Fe(ClO$_4$)$_2$·6H$_2$O (0.36 g, 1.0 mmol). The resulting purple solution was stirred for 15 min under an argon atmosphere. The purple solid product was obtained by cooling, filtration, and subsequent drying under vacuum (yield 78%). Purple-blue plate-shaped crystals were obtained by vapor diffusion of Et$_2$O into an acetone solution after 2 days; these crystals contained a mixture of occluded acetone and diethyl ether, which could be observed in ^{1}H NMR of the crystals: FT-IR (KBr, cm^{-1}) ν(CO) 1679, ν_{asym}(COO) 1606, ν_{sym}(COO) 1452; absorption spectrum (CH$_3$CN) λ_{max}, nm (ϵ_M, M^{-1} cm^{-1}) 370 (2400), 544 (br, 690), 590 (sh, 600). Anal. Calcd for C$_{29}$H$_{29}$ClFeN$_4$O$_7$: C, 54.69; H, 4.59; N, 8.80; Cl, 5.57. Found: C, 54.44; H, 4.76; N, 8.65; Cl, 5.39. *Caution: Perchlorate salts are potentially explosive and should be handled with care.*

[Fe^{II}(TPA)(BF)](ClO$_4$) (2). A methanol solution of TPA·3HClO$_4$ (0.59 g, 1.0 mmol), 3.0 equiv of triethylamine (0.30 g, 3.0 mmol), and sodium benzoylformate (0.17 g, 1.0 mmol) was added to 1 equiv of Fe(ClO$_4$)$_2$·6H$_2$O (0.36 g, 1.0 mmol). The resulting yellow solution was stirred for 15 min under an argon atmosphere. The solid product was obtained by cooling and subsequent filtration. Upon drying under vacuum, the yellow solid turned green (yield 85%). Dissolution of this green solid in methanol yielded a pale yellow solution. Bright yellow block-shaped crystals were obtained by vapor diffusion of Et$_2$O into a methanol solution after 3 days: FT-IR (Nujol, cm^{-1}) ν(CO) 1678, ν_{asym}(COO) 1602, ν_{sym}(COO) 1444; absorption spectrum (CH$_3$CN) λ_{max}, nm (ϵ_M, M^{-1} cm^{-1}) 385 (2400); (CH$_2$Cl$_2$) 374 (1300), 552 (sh, 270), 606 (br, 280). Anal. Calcd for C$_{26}$H$_{23}$ClFeN$_4$O$_7$: C, 52.50; H, 3.90; N, 9.42. Found: C, 52.54; H, 4.17; N, 9.18.

[Fe^{II}(6TLA)(X-BF)](ClO$_4$) (X = *m*-NO$_2$, *p*-Cl, *p*-F, *p*-CH$_3$, *p*-OCH$_3$). Complexes with substituted BF were prepared by using the same experimental procedures outlined for **1**, but with phenyl-substituted benzoylformates in place of the parent benzoylformate. Elemental analysis results: ([Fe^{II}(6TLA)(*m*-NO$_2$-BF)](ClO$_4$)·H$_2$O) Anal. Calcd for C$_{29}$H$_{30}$ClFeN$_5$O$_{10}$: C, 49.77, H, 4.32, N, 10.00, Cl, 5.07. Found: C, 50.02, H, 4.57, N, 9.66, Cl, 4.91. ([Fe^{II}(6TLA)(*p*-Cl-BF)]-(ClO$_4$)) Anal. Calcd for C$_{29}$H$_{28}$Cl$_2$FeN$_4$O$_7$: C, 51.89, H, 4.20, N, 8.35, Cl, 10.56. Found: C, 51.64, H, 4.48, N, 8.15, Cl, 10.33. ([Fe^{II}(6TLA)-(*p*-F-BF)](ClO$_4$)·H$_2$O) Anal. Calcd for C$_{29}$H$_{30}$ClFFeN$_4$O$_8$: C, 51.77, H, 4.49, N, 8.33, F, 2.82. Found: C, 51.60, H, 4.70, N, 8.25, F, 2.73. ([Fe^{II}(6TLA)(*p*-CH$_3$-BF)](ClO$_4$)·H$_2$O·CH$_3$OH) Anal. Calcd for C$_{31}$H$_{37}$-ClFeN$_4$O$_9$: C, 53.12, H, 5.32, N, 7.99, Cl, 5.06. Found: C, 53.03, H, 5.34, N, 8.19, Cl, 5.21. ([Fe^{II}(6TLA)(*p*-OCH$_3$-BF)](ClO$_4$)) Anal. Calcd for C$_{30}$H$_{31}$ClFeN$_4$O$_8$: C, 54.03, H, 4.69, N, 8.40, Cl, 5.32. Found: C, 53.86, H, 4.73, N, 8.19, Cl, 5.49.

[Fe^{II}(6TLA)(PP)](ClO$_4$) (3). The preparation of **3** was analogous to that of **1**, but with the use of sodium phenylpyruvate instead of sodium benzoylformate: absorption spectrum (CH$_3$CN) λ_{max}, nm (ϵ_M, M^{-1} cm^{-1}) 326 (2700), 370 (sh, 1900). (3·H$_2$O) Anal. Calcd for C$_{30}$H$_{33}$ClFeN$_4$O$_8$: C, 53.87, H, 4.97, N, 8.38. Found: C, 53.95, H, 5.08, N, 8.19.

(9) Cooper, A. J. L.; Ginos, J. Z.; Meister, A. *Chem. Rev.* **1983**, *83*, 321−358.

(10) Siegel, B.; Lanphear, J. *J. Am. Chem. Soc.* **1979**, *101*, 2221−2222.

(11) Chiou, Y.-M.; Que, L., Jr. *J. Am. Chem. Soc.* **1992**, *114*, 7567−7568.

(12) Da Mota, M. M.; Rodgers, J.; Nelson, S. M. *J. Chem. Soc. A* **1969**, 2036−2044.

(13) Gafford, B. G.; Holwerda, R. A. *Inorg. Chem.* **1989**, *28*, 60−66.

(14) Nimitz, J. S.; Mosher, H. S. *J. Org. Chem.* **1981**, *46*, 211−213.

α-*Keto Acid-Dependent Non-heme Iron Enzymes*

J. Am. Chem. Soc., Vol. 117, No. 14, 1995 4001

Table 1. X-ray Diffraction Data of [Fe^{II}(6TLA)(BF)](ClO$_4$) (**1**) and [Fe^{II}(TPA)(BF)(MeOH)](ClO$_4$)·2MeOH (**2**·MeOH)

	1	**2·MeOH**
formula	C$_{29}$H$_{29}$ClFeN$_4$O$_7$	C$_{29}$H$_{35}$ClFeN$_4$O$_{10}$
fw (g mol^{-1})	636.88	690.92
crystal system	triclinic	orthorhombic
space group	P$\bar{1}$ (no. 2)	Pca2$_1$ (no. 29)
a (Å)	8.931(6)	19.875(6)
b (Å)	13.366(7)	8.916(4)
c (Å)	15.160(7)	18.02(1)
α (deg)	75.92(4)	90.00
β (deg)	81.06(5)	90.00
γ (deg)	70.78(5)	90.00
V (Å^3)	1652(4)	3193(4)
Z	2	4
ϱ_{calcd} (g cm^{-3})	1.281	1.438
crystal dimensions (mm)	0.60 × 0.45 × 0.10	0.55 × 0.30 × 0.12
radiation, λ (Å)	Mo Kα, 0.710 69	Mo Kα, 0.710 69
temperature (°C)	−101	−101
μ (cm^{-1})	5.89	6.12
2θ$_{max}$ (deg)	51.9	50.0
no. of rflns collected	7074	2906
no. of unique rflns	6481	2173
no. of unique rflns used	3556 (I > 3.00σ(I))	2173 [I > 2.00σ(I)]
no. of least sq params	403	405
R^a	0.071	0.054
R$_w$^{a}	0.082	0.056

^{a} $R = \sum||F_o| - |F_c||/\sum|F_o|$; $R_w = [(\sum w(|F_o| - |F_c|)^2/\sum wF_o^2]^{1/2}$, where $w = 4F_o^2/[\sigma^2(F_o^2)]$ and $\sigma^2(F_o^2) = [S^2(C + R^2B) + (pF_o^2)^2]/(Lp^2$ with S = scan rate, C = total integrated peak count, R = ratio of scan time to background counting time, B = total background count, Lp = Lorentz-polarization factor, and $p = p$ factor (0.05).

[Fe^{II}(5TLA)(BF)](BPh$_4$) (4). The preparation was similar to that of **1**, but with the use of 5TLA in place of 6TLA, and the yellow solid was obtained by metathesis with NaBPh$_4$. Anal. Calcd for C$_{53}$H$_{49}$-BFeN$_4$O$_3$: C, 74.31, H, 5.77, N, 6.54. Found: C, 74.12, H, 6.00, N, 6.46.

X-ray Crystallography. A purple-blue plate-shaped crystal of **1** and a bright yellow block-shaped crystal of **2·MeOH** were mounted on glass fibers with heavy-weight oil and quickly placed under a cold N$_2$ stream on the diffractometer. Measurements were carried out on an Enraf-Nonius CAD-4 diffractometer with graphite-monochromated Mo Kα (λ = 0.710 69 Å) radiation. Cell constants were obtained from a least-squares refinement of the setting angles for 25 reflections (22.3° < 2θ < 42.6°) for **1** and 24 reflections (29.4° < 2θ < 36.2°) for **2**. The stability of the crystals was monitored during data collection by measuring the intensities of three control reflections after every 75−80 min of exposure time. No significant decay in these intensities was observed during the course of data acquisition. Lorentz and polarization corrections were applied to the data, and absorption corrections based on ω scans were carried out to a maximum 2θ value of 51.9° for **1** and 50.0° for **2**.

Each structure was solved by direct methods using the TEXSAN crystallographic software package of the Molecular Structure Corp. Neutral atom scattering factors and anomalous dispersion terms were taken from a standard source.[15] All non-hydrogen atoms were refined with anisotropic thermal parameters, with the exception of the distinguishable but disordered solvent atoms in **1**. Hydrogen atoms were included as a fixed contribution to F_c at their calculated positions (C−H = 0.95 Å). Some disorder in the solvent molecule was encountered during the refinement of the structure of **1** but was not modeled. As indicated by ^{1}H NMR, both acetone and ether were present in the crystal, which accounted for the electron density in this area. No disorder was found in the crystal of **2·MeOH**. The maximum and minimum peaks on the final difference Fourier maps corresponded to +0.91 and −0.70 e/Å^3 and +0.38 and −0.44 e/Å^3 for **1** and **2**, respectively.

Crystal data, together with details of the diffraction experiment and subsequent calculations, are summarized in Table 1. Selected bond

(15) Cromer, D. T.; Waber, J. T. *International Tables for X-ray Crystallography*; Kynoch Press: Birmingham, England, 1974; Vol. IV.

Table 2. Selected Bond Lengths and Angles for [Fe^{II}(6TLA)(BF)](ClO$_4$) (**1**)^a

a. Bond Lengths (Å)			
Fe1−O1	2.001(4)	Fe1−O2	2.212(4)
Fe1−N1	2.171(5)	Fe1−N11	2.273(6)
Fe1−N21	2.166(5)	Fe1−N31	2.231(6)
O1−C1	1.281(7)	O2−C2	1.234(7)
O3−C1	1.211(7)	C1−C2	1.541(9)
C2−C3	1.541(9)		

b. Bond Angles and Torsion Angles (deg)			
O1−Fe1−O2	75.3(2)	O1−Fe1−N11	101.9(2)
O1−Fe1−N21	118.7(2)	O1−Fe1−N31	103.5(2)
O2−Fe1−N1	84.7(2)	O2−Fe1−N11	88.7(2)
O2−Fe1−N31	89.6(2)	N1−Fe1−N11	77.2(2)
N1−Fe1−N21	81.3(2)	N1−Fe1−N31	76.0(2)
N11−Fe1−N21	85.4(2)	N21−Fe1−N31	89.9(2)
Fe1−O1−C1	121.8(4)	Fe1−O2−C2	113.6(4)
O1−C1−C2	112.2(5)	O2−C2−C1	116.6(6)
Fe1−O1−C1−O3	−175.5(6)	Fe1−O1−C1−C2	3.7(7)
O1−C1−C2−O2	2.3(8)	O1−C1−C2−C3	−176.5(6)

^{a} Estimated standard deviations in the least significant figure are given in parentheses.

Table 3. Selected Bond Lengths and Angles for [Fe^{II}(TPA)(BF)(MeOH)](ClO$_4$)·2MeOH (**2·MeOH**)^a

a. Bond Lengths (Å)			
Fe1−O1w	2.137(6)	Fe1−O1	2.014(6)
Fe1−N1	2.220(7)	Fe1−N11	2.170(7)
Fe1−N21	2.218(7)	Fe1−N31	2.130(7)
O1w−C1w	1.45(1)	O1−C1	1.27(1)
O2−C2	1.20(1)	O3−C1	1.22(1)
C1−C2	1.53(1)	C2−C3	1.51(1)

b. Bond Angles and Torsion Angles (deg)			
O1w−Fe1−O1	97.5(2)	O1w−Fe1−N1	97.4(3)
O1w−Fe1−N11	88.2(2)	O1w−Fe1−N31	86.0(2)
O1−Fe1−N11	99.0(3)	O1−Fe1−N21	87.9(2)
O1−Fe1−N31	107.4(3)	N1−Fe1−N11	78.1(3)
N1−Fe1−N21	76.9(3)	N1−Fe1−N31	77.0(3)
N11−Fe1−N21	81.8(3)	N21−Fe1−N31	101.2(3)
Fe1−O1w−C1w	130.2(5)	Fe1−O1−C1	141.7(6)
O1−C1−O3	126.2(8)	O1−C1−C2	118.2(7)
O2−C2−C1	118.9(8)	O1−C1−C2−O2	75(1)
Fe1−O1−C1−O3	−176.1(6)	Fe1−O1−C1−C2	9(1)

^{a} Estimated standard deviations in the least significant figure are given in parentheses.
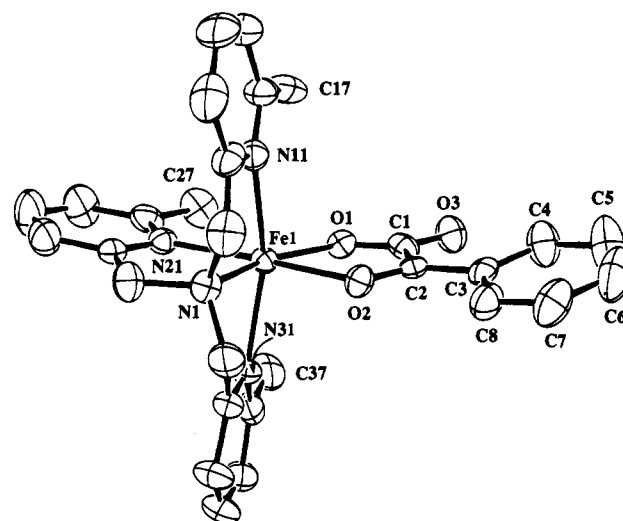
Figure 1. ORTEP view of [Fe^{II}(6TLA)(BF)]$^+$ (**1**), showing 50% probability thermal ellipsoids. Hydrogen atoms are omitted for clarity.

lengths and angles for **1** and **2** are listed in Tables 2 and 3; the ORTEP plots of [Fe^{II}(6TLA)(BF)]$^+$ and [Fe^{II}(TPA)(BF)(MeOH)]$^+$ are shown in Figures 1 and 2, respectively. The ORTEP plots with complete
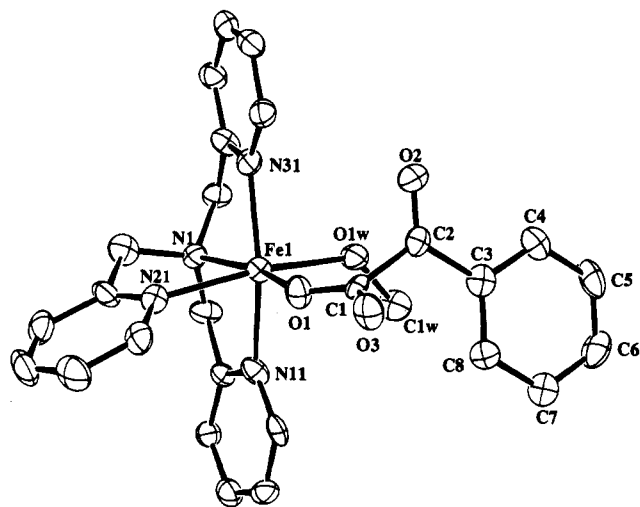
Figure 2. ORTEP view of [Fe^{II}(TPA)(BF)(MeOH)]$^+$ (2·MeOH), showing 50% probability thermal ellipsoids. Hydrogen atoms are omitted for clarity.

labeling schemes, tables of atomic positional parameters, final thermal parameters, and bond lengths and angles are supplied as supplementary material.

Physical Methods. Room-temperature electronic absorption spectra were recorded in 1-cm quartz cuvettes on a Hewlett-Packard 8451 diode array spectrophotometer (190−820-nm scan range). IR spectra were obtained with a Perkin-Elmer 1600 Series FT-IR instrument. ^{1}H and ^{13}C NMR spectra were recorded on a Varian VXR-300 or an IBM AC-300 spectrometer at room temperature. All spectra were obtained using a 90° pulse with 16K data points. Samples of iron complexes were made in CD$_3$CN or CDCl$_3$ at concentrations ranging from 5 to 10 mM. Chemical shifts (ppm) for complexes were referenced to the residual protic solvent peak. An inversion-recovery pulse sequence (180°−τ−90°−AQ) was used to obtain nonselective proton longitudinal relaxation times (T_1) with the carrier frequency set at several different positions to ensure the validity of the measurements. ^{31}P NMR spectral data, obtained with proton decoupling, were used to determine the yields of OPPh$_3$, which were calculated by integration relative to PPh$_3$, on the basis of calibrations with authentic samples of known concentrations.

Electrochemical measurements were carried out under argon at ambient temperature in solutions of CH$_3$CN with 0.1 M tetraethylammonium perchlorate as the supporting electrolyte using a BAS 100 electrochemical analyzer. Cyclic voltammograms (CV) were obtained by using a three-component system consisting of a platinum disk working electrode, a platinum wire auxiliary electrode, and a BAS saturated calomel reference electrode. The ferrocenium/ferrocene couple was measured under the same conditions to correct for junction potentials.

Ligands and isolated organic products were analyzed by electron impact mass spectrometry (EI-MS; 70 eV). Iron complexes were analyzed by fast atom bombardment mass spectrometry (FAB-MS) experiments using a 7070E-HF high-resolution double-focusing mass spectrometer equipped with a VG 11/250 data system (VG Analytical, Ltd.). An o-nitrophenyl octyl ether (ONPOE) matrix was used. Spectra were analyzed by comparison with isotopic ion distributions calculated via the ISO program of VG Analytical, Ltd. Calibration was checked before and after acquisition of data with a maximum error of ±0.3 Da. All FAB-MS samples were dissolved in acetonitrile.

HPLC analyses were obtained with a Waters 6000A solvent delivery system and a Waters U6K injector under isocratic conditions with a flow rate of 1 mL/min using a Whatman Partisil ODS-5 C18 10-μL reversed-phase column (25 × 4.6 cm). The UV detector for monitoring the products was set at 254 nm. Product analyses were also performed using a Perkin-Elmer Sigma 3 gas chromatograph equipped with a flame-ionization detector.

Oxygenation and Reactivity Studies. In a typical reaction, 1 (64 mg, 0.10 mmol) or 2 (60 mg, 0.10 mmol) was reacted with O$_2$ in 20 mL of CH$_3$CN under ambient conditions. After the reaction was complete, as indicated by the loss of color (1 week for 1) or as

monitored by HPLC analysis (2 days for 2), the reaction mixtures were submitted for FAB-MS analysis without further workup. Positive ion FAB-MS analysis of the oxygenated products of 1 and 2 gave an m/z 519 species, corresponding to [Fe^{II}(6TLA)(OBz)]$^+$ (5), and an m/z 1049 species, corresponding to [Fe^{III}$_2$(O)(TPA)$_2$(OBz)$_2$](ClO$_4$)$^+$ (6), respectively. Simulations of all isotopic combinations for these molecular ions gave isotopic distribution patterns that closely matched the observed patterns.

To extract organic product (benzoic acid) from the reaction mixtures, the solution was concentrated under reduced pressure. The residue was acidified with 10 mL of 3 N HCl to decompose the metal complexes. The organic product was extracted with diethyl ether (4 × 10 mL), dried over anhydrous Na$_2$SO$_4$, and concentrated. The extract was then submitted for EI-MS analysis or subjected to a reversed-phase isocratic HPLC separation, with a solvent mixture consisting of 5% HOAc/CH$_3$-OH/H$_2$O (25:50:25). m-Chlorobenzoic acid was added as an internal standard for the quantification of yields. Retention times and yields of products were confirmed by injection and comparison with authentic compounds. Yields of benzoic acid from the oxygenation reaction of 1 and 2 were 95% and 93%, respectively. ^{18}O-labeling experiments were run under analogous conditions in the presence of ^{18}O$_2$ or trace amounts (10 μL) of H$_2$^{18}O. The isotopic distribution values from the FAB-MS of the product complexes (5 and 6) and the EI-MS for their isolated organic products are listed in Table 6.

Reactions with 2,4-Di-*tert*-butylphenol. Solid 2,4-di-*tert*-butylphenol (45 mg, 0.5 mmol) was added to 1 (32 mg, 0.05 mmol) or 2 (30 mg, 0.05 mmol) in 20 mL of CH$_3$CN under an O$_2$ atmosphere at room temperature. The purple-blue color of 1 was retained after the addition of 2,4-di-*tert*-butylphenol. As the reaction proceeded, the color gradually turned yellow-brown over 4 days. The pale yellow solution of 2 turned green and then blue immediately upon the addition of 2,4-di-*tert*-butylphenol, and gradually turned yellow-brown over 2 days; the reaction of 2 was quenched after 2 days. The reaction mixtures were dried under vacuum and filtered through a silica gel column using Et$_2$O as eluent, giving 4,4′,6,6′-tetra-*tert*-butyl-2,2′-biphenol as judged by ^{1}H NMR (CCl$_4$): δ 1.33 (s, 18H), 1.42 (s, 18H), 5.16 (s, 2H), 6.96 (d, J = 2.5 Hz, 2H), 7.26 (d, J = 2.5 Hz, 2H). The relative amounts of starting phenol substrate and biphenol product were determined by ^{1}H NMR, and the yields were calculated on the basis of the starting Fe(II) complexes (75% and 100% for complexes 1 and 2, respectively).

Control experiments were also carried out in an anaerobic glovebox with deoxygenated CH$_3$CN as solvent (to exclude O$_2$ from the reactions) or in an O$_2$ atmosphere without the presence of iron complexes. In neither of these experiments was biphenol formed.

Reactions with Triphenylphosphine. Triphenylphosphine (130 mg, 0.5 mmol) was added to 1 (64 mg, 0.10 mmol) or 2 (60 mg, 0.10 mmol) in 20 mL of CH$_3$CN under an O$_2$ atmosphere at room temperature. Reaction mixtures of 1 and 2 were quenched after 4 and 2 days, respectively, and dried under vacuum; organic products were extracted with 10% EtOH/Et$_2$O (v/v) and filtered through a silica gel column. The amounts of OPPh$_3$ formed were determined by ^{31}P NMR integrations (61% for 1 and 68% for 2); the values were corrected by values from control experiments run in the absence of metal complexes.

Kinetic Measurements. Kinetic measurements were carried out using a Cary 14 spectrophotometer interfaced with a computerized data acquisition system with temperature controlled at 30.0 ± 0.1 °C. The observed rate constants were obtained from an exponential fit of the raw data utilizing a data processing program developed by the OLIS Corp. The acetonitrile solvent was saturated with oxygen gas at atmospheric pressure for approximately 1 h prior to use ([O$_2$] = 8.1 ± 0.6 mM at 25 °C).[16] Samples of [Fe^{II}(6TLA)(X-BF)](ClO$_4$) (0.3−0.5 mM scale) were placed in a cylindrical cuvette with a 5-cm path length. In all cases, at least a 10-fold stoichiometric excess amount of dioxygen over the iron(II) complexes was present in solution to ensure pseudo-first-order conditions. The oxygenation kinetics were followed by monitoring the disappearance of the low-energy iron(II)-to-α-ketocarboxylate charge-transfer (MLCT) transition bands of the complexes. Each rate constant was an average of 3−5 trials. The kinetic results are listed in Table 4.
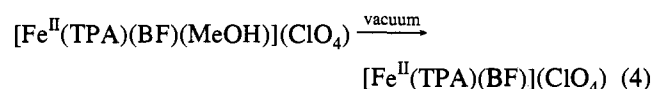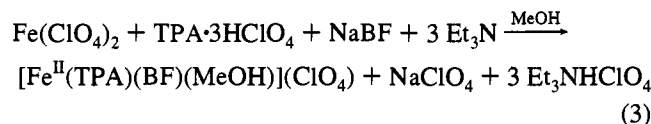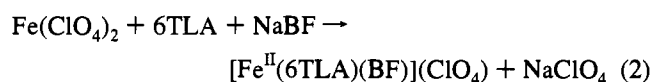
(16) Achord, J. M.; Hussey, C. L. *Anal. Chem.* **1980**, *52*, 601−602.

Table 4. UV−Vis Absorption Properties of
[Fe^{II}(6TLA)(X-BF)](ClO$_4$) Complexes and Kinetic Data for Their
Oxidative Decarboxylation Reactions[a]

X	λ_{max}[b] (ϵ[c])		E_{max}[d]	σ[e]	k_{obs}[f]
m-NO$_2$	360 (1500)	570 (420)	17 540	0.71	7.65(3)
p-Cl	370 (1400)	554 (400)	18 050	0.24	1.95(2)
p-F	366 (1400)	542 (370)	18 450	0.15	1.211(1)
H	385 (2400)	544 (690)	18 380	0.00	1.043(4)
p-CH$_3$	368 (2400)	536 (690)	18 660	−0.14	0.965(3)
p-OCH$_3$	324 (15 000)	532 (550)	18 800	−0.28	0.616(5)

[a] In CH$_3$CN. [b] Units of nm. [c] Units of M^{-1} cm^{-1}. [d] Energy of λ_{max}
of LMCT bands, units of cm^{-1}. [e] Hammett substituent constants.
[f] Measured at 30.0 ± 0.1 °C, units of 10^{-3} min^{-1}.

Results and Discussion

Syntheses. To explore the chemistry of iron(II)−α-ketocar-
boxylate complexes and their reactions with dioxygen, we have
synthesized the first 1:1 complexes of iron(II) and α-keto acids,
with tetradentate tripodal ligands 6TLA, TPA, or 5TLA
comprising the remainder of the coordination sphere. Treatment
of Fe(ClO$_4$)$_2$·6H$_2$O with an equimolar quantity of tripodal 6TLA
ligand and benzoylformate in methanol under argon gave a
purple-blue solution that, after workup, afforded [Fe^{II}(6TLA)-
(BF)](ClO$_4$) (**1**) (eq 2). The use of TPA in place of 6TLA
yielded a yellow solid, [Fe^{II}(TPA)(BF)(MeOH)](ClO$_4$) (**2·MeOH**),
which turned green upon drying under vacuum (eqs 3 and 4).

$$Fe(ClO_4)_2 + 6TLA + NaBF \longrightarrow$$
$$[Fe^{II}(6TLA)(BF)](ClO_4) + NaClO_4 \quad (2)$$

$$Fe(ClO_4)_2 + TPA\cdot 3HClO_4 + NaBF + 3\ Et_3N \xrightarrow{MeOH}$$
$$[Fe^{II}(TPA)(BF)(MeOH)](ClO_4) + NaClO_4 + 3\ Et_3NHClO_4 \quad (3)$$

$$[Fe^{II}(TPA)(BF)(MeOH)](ClO_4) \xrightarrow{vacuum}$$
$$[Fe^{II}(TPA)(BF)](ClO_4) \quad (4)$$

In order to investigate the electronic factors that affect the
spectroscopic and reactivity properties of these complexes, a
series of 6TLA complexes with meta- or para-substituted
benzoylformic acids were synthesized. [Fe^{II}(6TLA)(PP)](ClO$_4$)
(**3**) and [Fe^{II}(5TLA)(BF)](ClO$_4$) (**4**) were also prepared for
similar reasons.

Description of Structures. [Fe^{II}(6TLA)(BF)](ClO$_4$), 1.
Recrystallization of **1** from acetone/Et$_2$O afforded purple-blue
crystals suitable for X-ray crystallography. The crystal structure
of **1** shows the iron in a distorted octahedron with a tetradentate
tripodal 6TLA ligand and a bidentate BF ligand, the α-keto acid
functionality and the N21 pyridine ring defining an approximate
plane of symmetry for the complex (Figure 1). Benzoylformate
is coordinated to the iron center via a carboxylate oxygen (O1)
at 2.001(4) Å and the carbonyl oxygen (O2) at 2.212(4) Å, the
0.21 Å bond length difference due to the greater basicity of the
carboxylate. The shorter Fe−O1 bond is trans to the weaker
Fe−N$_{amine}$ bond, and the longer Fe−O2 bond is trans to the
stronger Fe−N$_{py}$ bond. The phenyl group is nearly coplanar
with the α-ketocarboxylate moiety, with a O1−C1−C2−O2
torsion angle of 2.3(8)°. The C−O bond lengths of the α-keto
acid moiety clearly indicate an electron-localized carboxylate
anion (O1−C1 = 1.281(7) Å and O3−C1 = 1.211(7) Å) singly
bonded (C1−C2 = 1.541(9) Å) to the α-carbonyl group (O2−
C2 = 1.234(7) Å). The O2−C2 bond is lengthened relative to
the O3−C1 carbonyl bond due to the binding of O2 to the iron
center.

Steric interactions between the C27 α-methyl group and the
C17 and C37 methyl grops of 6TLA ligand prevent the axial
pyridine nitrogens from coordinating to the iron(II) center at
the optimum bond length, and result in longer axial Fe−N11
and Fe−N31 distances than the equatorial Fe−N1 and Fe−N21
distances. Furthermore, the O1−Fe−N21 angle (118.7(2)°) is
significantly larger than the ideal 90° octahedral angle. Such
distortions from octahedral geometry are typical of the 6TLA
ligand and have also been observed in [Fe^{II}$_2$(6TLA)$_2$F$_2$](BF$_4$)$_2$[17]
and [Fe^{II}(6TLA)(OBz)](BPh$_4$) (**5**).[18] The structures of com-
plexes **1** and **5**, in particular, are comparable; as in **1**, the
bidentate benzoate in **5** is unsymmetrically chelated to the high-
spin iron(II) center. The bond angle between the benzoate
oxygen and the coplanar pyridine nitrogen is even larger
(125.07(8)°) than the corresponding O1−Fe−N21 angle of **1**
(118.7(2)°).

[Fe^{II}(TPA)(BF)(MeOH)](ClO$_4$)·2MeOH, 2·MeOH. Com-
plex **2·MeOH** is also a distorted octahedron featuring a tet-
radentate TPA, a monodentate BF, and a methanol in the
coordination sphere (Figure 2). Besides the iron-bound metha-
nol (Fe−O1w = 2.137(6) Å), two solvate methanol molecules
are also found per molecular unit in the crystal lattice. The BF
ligand is coordinated to the iron center only via its carboxylate
oxygen (O1) at 2.014(6) Å from the iron. The carbonyl oxygen
(O2) of BF is not bound to the iron. As a result, the α-keto
acid moiety is no longer planar, the torsion angle between the
carboxylate and the carbonyl of BF, i.e., O1−C1−C2−O2,
being 75(1)°. Furthermore, the BF phenyl ring is also rotated
out of conjugation with the α-keto acid function.

The tripodal TPA ligand occupies the remaining coordination
sites on the iron(II) center and adopts the characteristic
configuration of such a tripod with N$_{amine}$−Fe−N$_{py}$ angles
averaging ~77° to accommodate the five-membered chelate
rings. Like **1**, the Fe−N$_{amine}$ bond is longer (2.220(7) Å) and
trans to the shorter Fe−O1 bond. The Fe−N$_{py}$ bond trans to
Fe−O1w is also longer (2.218(7) Å) than the other two, which
are trans to each other (2.170(7) and 2.130(7) Å). These values
observed for **2** are comparable with other TPA complexes,[19−22]
particularly [Fe^{II}$_2$(TPA)$_2$(OAc)$_2$](BPh$_4$)$_2$[23] and [Fe^{II}$_2$(TPA)$_2$Cl$_2$]-
(BPh$_4$)$_2$.[17]

The major difference between 6TLA and TPA complexes is
the relative lengths of the various Fe−N bonds. In TPA
complexes, the two pyridine nitrogen atoms trans to each other
have shorter Fe−N distances than the other two Fe−N bonds,
while in the 6TLA complexes, due to steric interactions arising
from the presence of the α-methyl groups, the two pyridine
nitrogen atoms trans to each other are pushed away from each
other and result in longer Fe−N bonds than the other two Fe−N
bonds. As a result of steric congestion, the iron center of **1**
cannot accommodate the binding of both the BF ligand and a
solvent molecule (as found in the structure of **2**), and the BF
carbonyl oxygen binds to the iron to compensate for the weak
ligand environment provided by the 6TLA ligand, which also

(17) Zang, Y.; Jang, H. G.; Chiou, Y.-M.; Hendrich, M. P.; Que, L., Jr.
Inorg. Chim. Acta **1993**, *213*, 41−48.

(18) Zang, Y.; Elgren, T. E.; Dong, Y.; Que, L., Jr. *J. Am. Chem. Soc.*
**1993**, *115*, 811−813.

(19) Jang, H. G.; Cox, D. D.; Que, L., Jr. *J. Am. Chem. Soc.* **1991**, *113*,
9200−9204.

(20) Norman, R. E.; Yan, S.; Que, L., Jr.; Backes, G.; Ling, J.; Sanders-
Loehr, J.; Zhang, J. H.; O'Connor, C. J. *J. Am. Chem. Soc.* **1990**, *112*,
1554−1562.

(21) Norman, R. E.; Holz, R. C.; Ménage, S.; O'Connor, C. J.; Zhang,
J. H.; Que, J. L. *Inorg. Chem.* **1990**, *29*, 4629−4637.

(22) Yan, S.; Cox, D. D.; Pearce, L. L.; Juarez-Garcia, C.; Que, L., Jr.;
Zhang, J. H.; O'Connor, C. J. *Inorg. Chem.* **1989**, *28*, 2507−2509.

(23) Ménage, S.; Zang, Y.; Hendrich, M. P.; Que, L., Jr. *J. Am. Chem.
Soc.* **1992**, *114*, 7786−7792.

4004 *J. Am. Chem. Soc., Vol. 117, No. 14, 1995*

Chiou and Que
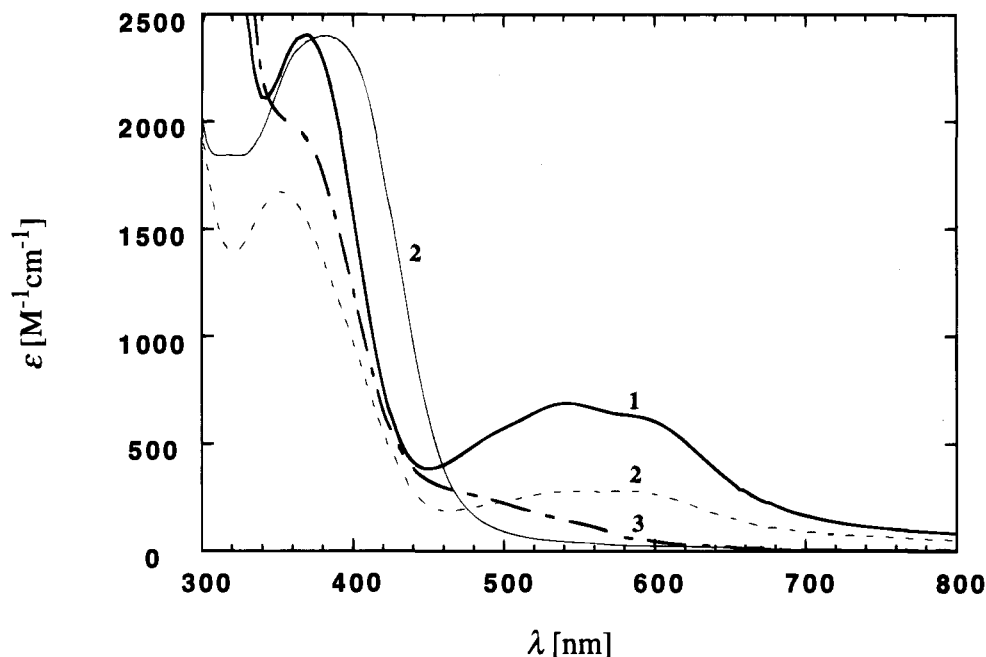
Figure 3. UV—vis absorption spectra of [Fe^{II}(6TLA)(BF)](ClO$_4$) (**1**; bold line), [Fe^{II}(6TLA)(PP)](ClO$_4$) (**3**; bold dotted line), and [Fe^{II}(TPA)(BF)]-(ClO$_4$) (**2**) in CH$_3$CN (plain line) and in CH$_2$Cl$_2$ (dotted line) at ambient temperature.
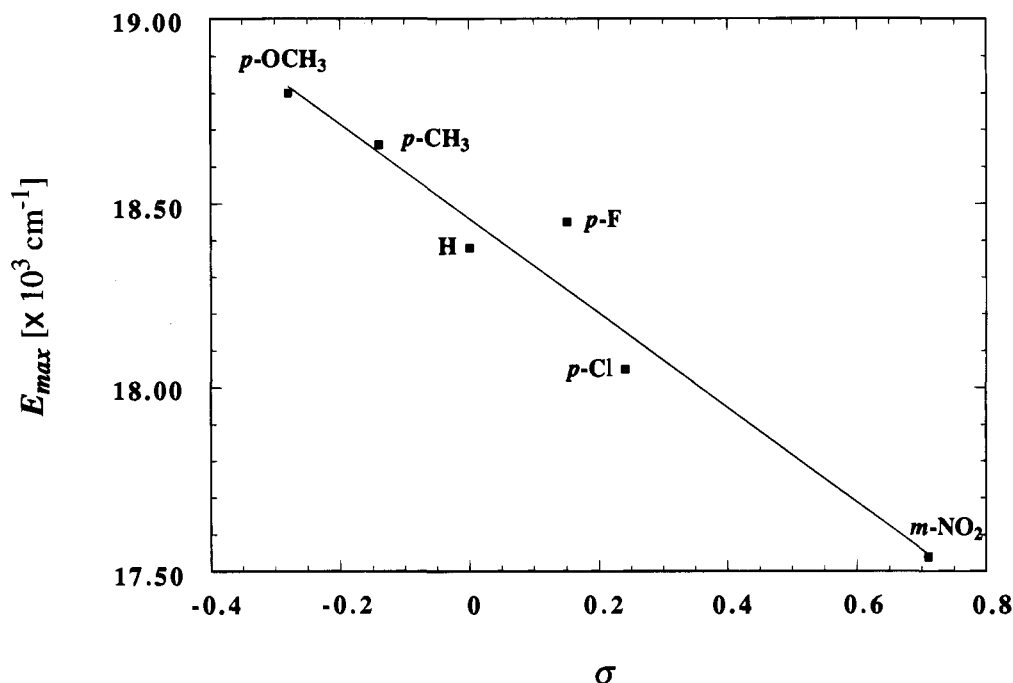
Figure 4. Energy of the λ_{max} of MLCT bands for [Fe^{II}(6TLA)(X-BF)](ClO$_4$) plotted versus the Hammett σ constants of the substituents in the benzoylformate part of the complexes. The line represents the following equation: E (cm^{-1}) = 1.85 × 10^4 − (1.28 × 10^3)σ (R^2 = 0.98).

results in a longer average Fe—N$_{py}$ bond (2.22 Å) for **1** than for **2** (2.17 Å). The O1—Fe1—O2 angle of 75.3(2)° in **1** is smaller than the corresponding O1w—Fe1—O1 angle of 97.5-(2)° in **2**, reflecting the smaller steric demands of the bidentate BF ligand in **1** relative to the two monodentate ligands in **2**.

Electronic Absorption Properties. The UV—vis spectra for complexes **1, 2**, and **3** are displayed in Figure 3. These spectra and those of a series of [Fe^{II}(6TLA)(X-BF)](ClO$_4$) complexes (Table IV) shed light on the nature of these transitions. The higher energy transitions (340—420 nm) are found for all complexes and assigned as charge-transfer transitions between the iron(II) ion and pyridines.[24] Complex **1** exhibits an unusual

(24) Borovik, A. S.; Papaefthymiou, V.; Taylor, L. F.; Anderson, O. P.; Que, L., Jr. *J. Am. Chem. Soc.* **1989**, *111*, 6183—6195.

purple-blue color associated with features at 544 nm (ϵ = 690 M^{-1} cm^{-1}) and 590 nm (sh, ϵ = 600 M^{-1} cm^{-1}) in CH$_3$CN. The absorption properties of **1** persist in both coordinating and noncoordinating solvents such as CH$_3$CN and CH$_2$Cl$_2$, respectively. When a series of ring-substituted BF ligands are used in place of BF in **1**, the corresponding complexes give rise to visible bands whose λ_{max} values shift to lower energies with more electron-withdrawing substituents (Table 4), suggesting that they have iron(II)-to-α-ketocarboxylate charge-transfer (MLCT) character. The energy of the band correlates with the Hammett σ constants of the substituents on the phenyl ring of the benzoylformate (Figure 4). The effects of the substituents are transmitted via conjugation within the approximately planar conformation adopted by the BF moiety when the α-keto group

is chelated to the iron. In contrast, $[Fe^{II}(6TLA)(PP)](ClO_4)$ (**3**), with phenylpyruvate in place of benzoylformate in **1**, is orange-red in CH_3CN with $\lambda_{max} = 326$ nm ($\epsilon = 2700$ M^{-1} cm^{-1}) and $\lambda_{sh} = 370$ nm ($\epsilon = 1900$ M^{-1} cm^{-1}), and no distinct visible transitions (Figure 3). The color difference between **1** and **3** indicates that the low-energy absorption features of **1** are related to the π conjugation within the BF ligand, since the methylene group of PP disrupts the conjugation between the phenyl group and the α-ketocarboxylate function in the BF ligand. Therefore, it can be concluded that the presence of the purple-blue color for the Fe(II)−BF complexes is indicative of a chelated α-ketocarboxylate to the iron with an approximately planar, conjugated phenyl group.

On the other hand, $[Fe^{II}(TPA)(BF)](ClO_4)$ (**2**) is yellow in CH_3CN ($\lambda_{max} = 385$ nm, $\epsilon = 2400$ M^{-1} cm^{-1}) and green in CH_2Cl_2 ($\lambda_{max} = 374$ nm, $\epsilon = 1700$ M^{-1} cm^{-1}, and broad bands between 550 and 610 nm, $\epsilon = 280$ M^{-1} cm^{-1}) (Figure 3). Similarly, $[Fe^{II}(5TLA)(BF)](BPh_4)$ (**4**) is yellow in CH_3CN ($\lambda_{max} = 380$ nm, $\epsilon = 2400$ M^{-1} cm^{-1}) and green in CH_2Cl_2 ($\lambda_{max} = 378$ nm, $\epsilon = 1700$ M^{-1} cm^{-1}, and broad bands between 560 and 620 nm, $\epsilon = 370$ M^{-1} cm^{-1}). The solvent-dependent phenomenon observed for **2** and **4** is very likely due to the two possible binding modes of the BF ligand. In the presence of coordinating CH_3CN or MeOH, BF is a monodentate ligand with a solvent molecule occupying the sixth site of the iron coordination sphere and **2** exhibits the typical light yellow color for high-spin iron(II)−TPA complexes.[17,23] In a noncoordinating solvent, BF chelates to the iron, giving rise to visible features similar to those of **1**. The lower extinction coefficients found for **2** and **4** in CH_2Cl_2 may indicate the presence of an equilibrium between chelated and monodentate forms of the BF ligand in noncoordinating solvents. These solvent effects on electronic spectra parallel the effects of various solvents on intramolecular hydrogen bonding of benzoylformic acid.[25] In noncoordinating solvents, benzoylformic acid adopts a nearly planar conformation with an intramolecular hydrogen bond between the carboxylic acid proton and the α-keto oxygen; this planar structure is disrupted in polar solvents due to intermolecular hydrogen bonding.

NMR Properties. Figures 5 and 6 show the ^1H NMR spectra of **1** and **2**, and their chemical shifts and those of other complexes of interest are collected in Table 5 along with their assignments. These assignments are based on comparisons with other Fe(II)−TPA complexes[23] and on peak integration and relaxation time (T_1) measurements. The number of pyridine peaks observed shows that the tripodal ligands have an effective 3-fold symmetry in solution, suggesting that the six-coordinate structures are in rapid equilibrium with trigonal bipyramidal structures having a monodentate BF ligand on the NMR time scale.

In the spectrum of **1** (Figure 5A), the py α-CH_3 protons are shifted upfield to −35 ppm and have the shortest T_1 value (0.60 ms), while the methylene protons are too broad to be observed. The β and β' protons on each pyridine (~5.0 and 5.3 Å from the iron) are resolved from each other and assigned to the 46- and 50-ppm peaks. The py γ protons are found at 16 ppm, almost overlapping with the para H of the BF ligand. The BF protons show relatively large downfield isotropic shifts (ortho H at 24 ppm, meta H at 11 ppm, and para H at 16 ppm) due to delocalization of unpaired spin density of the iron through the chelated α-ketocarboxylate onto the coplanar, π-conjugated phenyl group. The assignments for the BF protons were confirmed by the connectivities observed in a COSY experi-

ment.[26,27] Similar shifts were observed for the 6TLA protons of **3**, but the phenyl protons of the PP ligand exhibit smaller downfield shifts due to the presence of the intervening CH_2 group.

The ^1H NMR spectra of **2** and **4** in $CDCl_3$ resemble that of **1** but differ from those of **2** and **4** in CD_3CN (Figure 6). In $CDCl_3$, the BF protons of **2** and **4** (denoted with asterisks in Figure 6B) display a similar pattern of chemical shifts as found in **1**, consistent with a chelated, planar BF ligand. These resonances are not as downfield shifted as those of **1** and may reflect a shift in the equilibrium between chelated and monodentate BF forms favoring the latter. Indeed, larger isotropic shifts are observed for complexes with more intense visible bands, consistent with the differing mole fractions of the chelated BF form in these complexes. On the other hand, the BF protons of **2** and **4** in CD_3CN are in the diamagnetic region (Figure 6A and Table V); nevertheless, they have relatively short T_1 values, indicating that the BF ligand remains coordinated to the high-spin iron(II) center.[28] The smaller isotropic shifts indicate that the coordinating solvent, occupying the sixth site of the iron coordination sphere, disrupts the delocalization of the unpaired spin density onto the phenyl ring of the BF ligand via the carbonyl oxygen by displacing the carbonyl oxygen of the BF ligand.

Electrochemistry. The redox properties of complexes **1**, **2**, and **4** were investigated by cyclic voltammetry (CV) experiments to gain insight into their reactivities. In acetonitrile with tetraethylammonium perchlorate as the supporting electrolyte, **1** exhibits an irreversible one-electron wave at +870 mV versus NHE, corresponding to the Fe^{III}/Fe^{II} couple, like the observation by Zang *et al.* for $[Fe^{II}(6TLA)(OBz)]^+$ (**5**).[18] Complexes **2** and **4** exhibit similarly irreversible waves, but with the Fe^{III}/Fe^{II} couples being shifted to +340 and +320 mV, respectively.

The CV results clearly demonstrate the effects of introducing methyl substituents on the pendant pyridines. The steric interactions of the α-methyl grops of 6TLA prevent the pyridine nitrogens from approaching the iron center as closely as in **1**, making 6TLA a weaker ligand; this stabilizes Fe(II) relative to Fe(III) and shifts the redox potential of the metal center to a more positive value. On the other hand, the TPA and 5TLA complexes exhibit similar redox potentials, indicating that the presence of β-methyl groups in 5TLA does not significantly affect the redox properties of the iron center. In fact, **2** and **4** share many similar physical properties, including ^1H NMR, UV−vis, and electrochemical properties, as well as their reaction rates toward dioxygen. Hence, it is apparent that the electrochemical differences between **1** and **2** are attributable to steric factors.

Similar steric effects were also observed for other complexes. Introduction of the 6-methyl groups on the pyridine rings of the bispicen or TPA ligands of $[L_2Mn^{III}_2(\mu\text{-}O)_2]^{2+}$ complexes shifts the IV/IV ↔ III/IV and III/IV ↔ III/III couples by approximately 0.4 V in the positive direction.[29] For diiron(II) complexes, O_2 binding to $[Fe^{II}_2(HPTP)(OBz)]^{2+}$ is irreversible, indicating that the diiron(III) state is strongly favored relative to the diiron(II) state,[30] but the presence of 6-methyl groups in

(25) Hirota, M.; Shinozaki, F. *Bull. Chem. Soc. Jpn.* **1969**, *42*, 2614−2617.

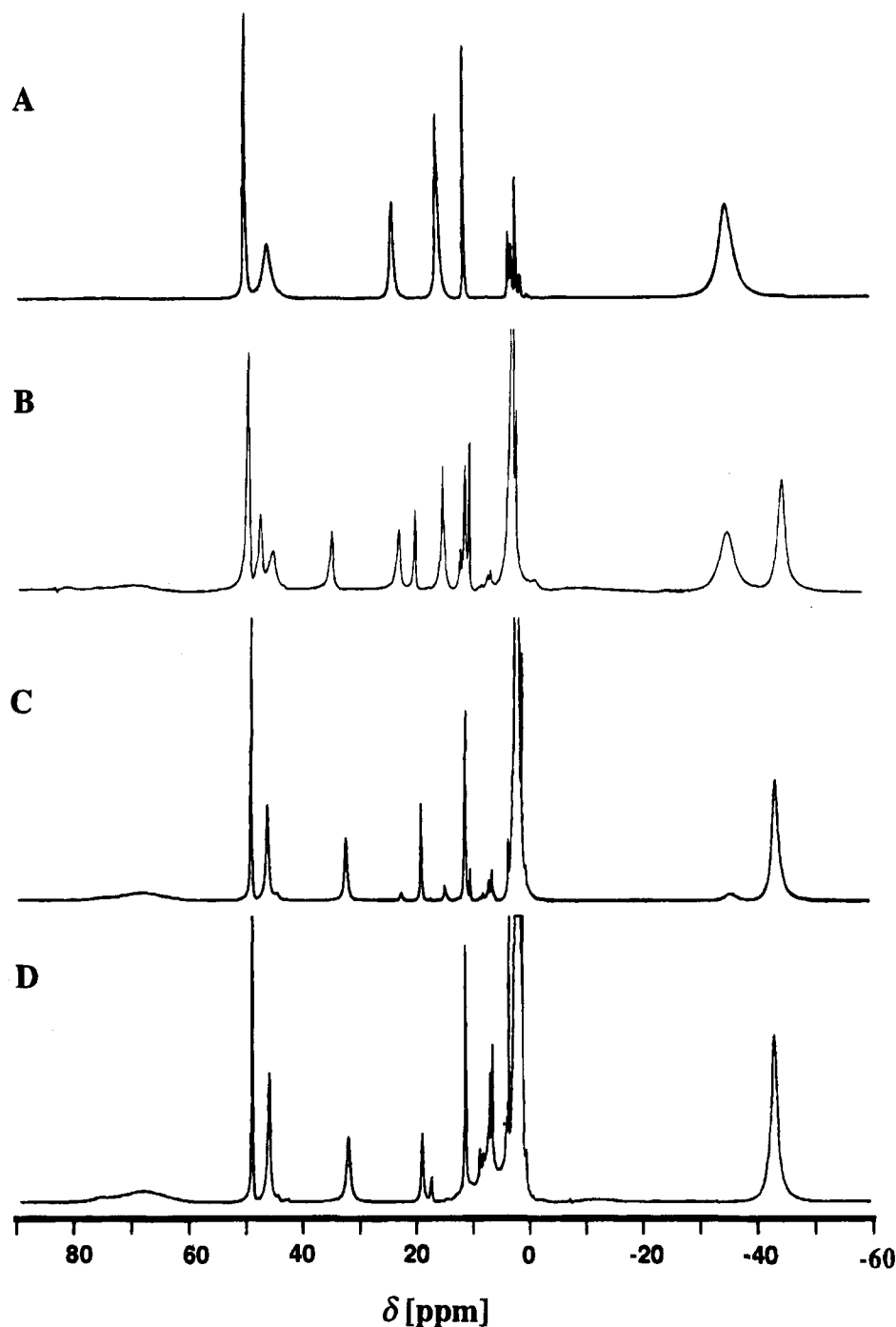(26) Ming, L.-J.; Jang, H. G.; Que, L., Jr. *Inorg. Chem.* **1992**, *31*, 359−364.

(27) Wang, Z.; Holman, T. R.; Que, L., Jr. *Magn. Reson. Chem.* **1993**, *31*, S78−S84.

(28) La Mar, G. N.; Horrocks, W. D., Jr.; Holm, R. H. *NMR of Paramagnetic Molecules, Principles and Applications*; Academic: New York, 1973.

(29) Goodson, P. A.; Oki, A. R.; Glerup, J.; Hodgson, D. J. *J. Am. Chem. Soc.* **1990**, *112*, 6248−6254.

(30) Dong, Y.; Ménage, S.; Brennan, B. A.; Elgren, T. E.; Jang, H. G.; Pearce, L. L.; Que, L., Jr. *J. Am. Chem. Soc.* **1993**, *115*, 1851−1859.

Figure 5. [^1]H NMR spectra of complex **1** in CD$_3$CN (A) and **1** incubated at 20 °C under an O$_2$ atmosphere for 2 days (B), 4 days (C), and 1 week (D).

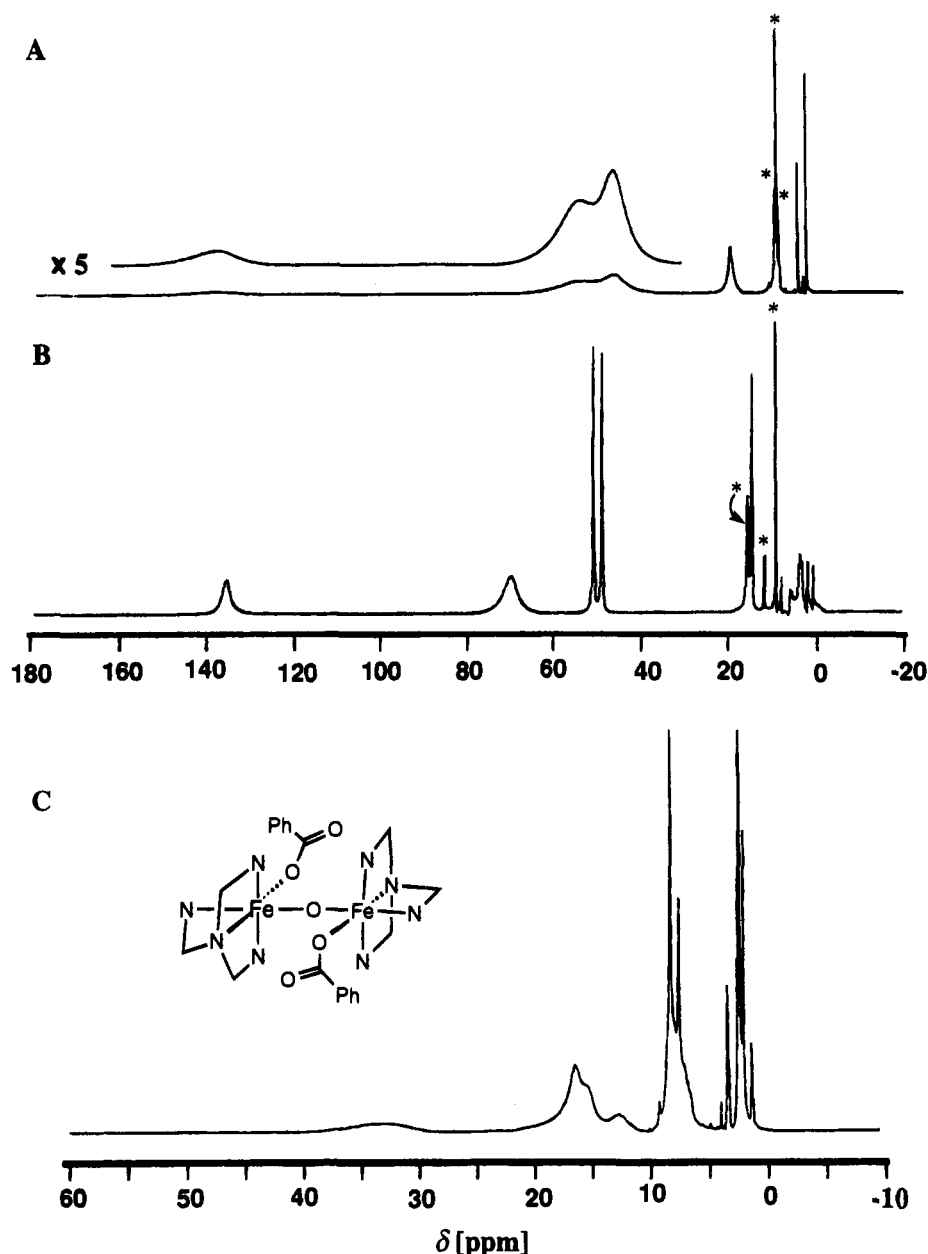[Fe^{II}$_2$(6-Me-HPTP)(OBz)]$^{2+}$ alters the balance between the diiron(II) and the diiron(III) states to favor reversibility.[31]

Reactivity with O$_2$. The reaction of the iron(II) center of α-keto acid-dependent enzymes with dioxygen is a key element of their function. Thus, the reactivity of synthetic model complexes with molecular oxygen is of great interest. Upon exposure to O$_2$, the purple-blue color of **1** in acetonitrile gradually fades and yields the oxidatively decarboxylated product [Fe^{II}(6TLA)(OBz)]$^+$ (**5**) in quantitative yield. This transformation can also be monitored by [^1]H NMR which shows that **1** completely converts over a period of 1 week to a new species (Figure 5) with features identical to those of independently prepared [Fe^{II}(6TLA)(OBz)](ClO$_4$) (**5**).[18] The shift of

(31) Hayashi, Y.; Suzuki, M.; Uehara, A.; Mizutani, Y.; Kitagawa, T. *Chem. Lett.* **1992**, *91–94*.

the α-CH$_3$ groups of the 6TLA ligand from −35 to −43 ppm is particularly useful for monitoring the conversion of the [Fe^{II}-(6TLA)(X-BF)](ClO$_4$) complexes to their corresponding [Fe^{II}-(6TLA)(X-OBz)](ClO$_4$) products, as the relative peak areas of the α-CH$_3$ groups can be integrated to determine the relative amounts of starting complex and product.

In contrast, **2** reacts with O$_2$ over a 2-day period as monitored by NMR and HPLC product analysis. The [^1]H NMR spectrum of the oxidation product **6** (Figure 6C) shows features only in the 0−40-ppm range attributed to the pyridine protons and suggests that it is a [Fe^{III}$_2$O(TPA)$_2$]-type complex, with a large antiferromagnetic coupling between the two paramagnetic centers.[20,22] The number of the TPA ligand resonances is indicative of the mode of TPA binding to the iron centers in these complexes. In the structurally characterized [Fe^{III}$_2$O-

Figure 6. ^{1}H NMR spectra of complex **2** in CD$_3$CN (A) and in CDCl$_3$ (B), with the BF protons denoted with asterisks. The oxygenation product of **2**, [Fe^{III}$_2$(O)(TPA)$_2$(OBz)$_2$]$^{2+}$ (**6**), in CD$_3$CN is shown in (C).

Table 5. ^{1}H NMR Parameters[a,b]

assignments	1	2	2[c]	3	4	4[c]	5	6
CH$_2$	d	53 (2.4)	69 (1.0)	d	57 (1.0)	74.8 (1.0)	68 (1.8)	33 (0.79)[h]
α-CH$_3$ or py α	−35 (0.60)	137 (1.1)	135 (0.58)	−36 (0.70)	141 (0.46)	134 (0.58)	−43 (1.5)	
py β, β'	50 (7.3)	46 (8.4)	50 (7.7)	50 (8.0)	50 (7.7)	52 (7.9)	49 (10)	16 (4.9)
	46 (3.0)		48 (10)	46 (3.2)	9.7 (22)[f]	4.9 (24)[f]		
py γ	16 (~17)[e]	20 (22)	14 (21)	16 (11)	19 (23)	10 (52)	11 (28)	7.8 (15)
BF ortho H	24 (2.4)	9.0 (4.5)	15 (4.5)	11 (3.9)	8.9 (6.8)	20 (5.1)	46 (2.3)[i]	12.4 (5.2)[i]
BF meta H	11 (15)	8.6 (32)	8 (39)	6.3 (27)[e]	8.3 (42)	7.8 (42)[g]	32 (4.3)[i]	7.1 (22)[i]
BF para H	16 (~17)[e]	8.2 (60)	11 (74)	6.3 (27)[e]	7.9 (92)	14 (104)	19 (41)[i]	−
PP CH$_2$				21 (2.1)				

[a] **1** = [Fe^{II}(6TLA)(BF)](ClO$_4$); **2** = [Fe^{II}(TPA)(BF)](ClO$_4$); **3** = [Fe^{II}(6TLA)(PP)](ClO$_4$); **4** = [Fe^{II}(5TLA)(BF)](BPh$_4$); **5** = [Fe^{II}(6TLA)(OBz)]$^+$; **6** = [Fe^{III}$_2$O(TPA)$_2$(OBz)$_2$]$^{2+}$. Numbers in parentheses are relaxation times (T_1) in milliseconds. Greek letters designate positions on pyridine rings, and ortho, meta, and para designate positions on the benzoylformate or benzoate. [b] In CD$_3$CN, unless stated otherwise. [c] In CDCl$_3$. [d] Too broad to be seen. [e] These two peaks are too close to measure separate relaxation times. [f] β-CH$_3$. [g] This peak overlaps with BPh$_4$ protons. [h] Protons of py α or CH$_2$. [i] Protons of OBz.

(TPA)$_2$(OBz)]$^{3+}$ complex, one TPA binds with a pyridine trans to the oxo bridge, while the other TPA binds with the amine trans to the oxo bridge. This inequivalence gives rise to four different pyridine ring environments and is reflected by the complexity of its NMR spectrum.[20] The spectrum of the

oxygenation product from **2** has fewer TPA features, clearly indicating a more symmetric complex. FAB-MS data for the product complex show a peak at *m/z* 1049 corresponding to the molecular ion of {[Fe^{III}$_2$O(TPA)$_2$(OBz)$_2$](ClO$_4$)}$^+$. By analogy with the results by Ménage *et al.*,[23] the spectrum of **6**

Scheme 1

$$[Fe^{II}(L)(BF)]^+ + 2 \underset{\text{OH}}{\bigbenzene} \xrightarrow[\text{CH}_3\text{CN}]{O_2} 2 \underset{\text{O}\cdot}{\bigbenzene} + [Fe^{18}O(L)(OBz)]^+ + CO_2$$
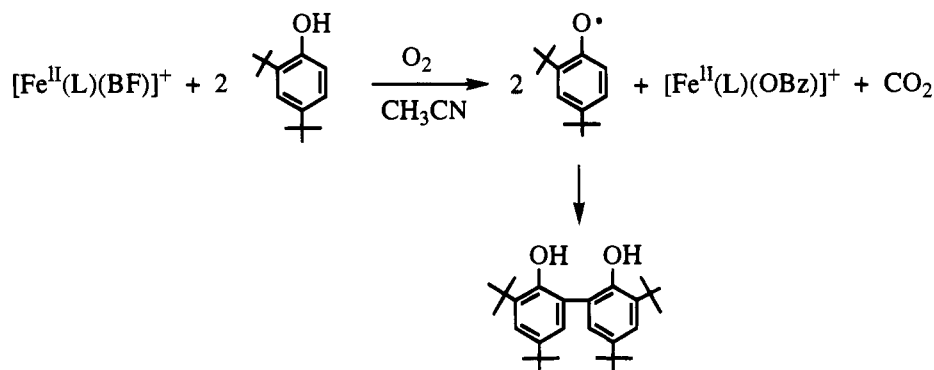
in Figure 6C is assigned to that of a (μ-oxo)diiron(III) complex with two terminal benzoates, i.e., $[Fe^{III}_2O(TPA)_2(OBz)_2]^+$. Two related structures were recently reported: $[Fe^{III}_2O(bipy)_4(CF_3-CO_2)_2]^{2+}$, wherein the two carboxylate ligands are terminally bound to the metal centers and the Fe−O−Fe angle is 163.0 (3)°,[32] and $[Fe^{III}_2O(TPA)_2Cl_2]^{2+}$, which has a linear Fe−O−Fe motif and the μ-oxo oxygen trans to two pyridine nitrogens of TPA.[33,34] The structure proposed for **6** (shown in Figure 6C) is similar to that of $[Fe^{III}_2O(TPA)_2Cl_2]^{2+}$, with an effective center of symmetry at the bridging oxygen.

The formation of this (μ-oxo)diiron(III) product complex likely results from a further autoxidation reaction of the initial oxidative decarboxylation product $[Fe^{II}(TPA)(OBz)]^+$, analogous to that observed for $[Fe^{II}_2(TPA)_2(OAc)_2]^{2+}$.[23] Such autoxidation reactions of iron(II) complexes are well documented for iron(II) porphyrins[35] and for some non-heme diiron-(II) compounds.[23,36] It is likely that the reaction of **2** with dioxygen proceeds first with the oxidative decarboxylation of its BF ligand, followed by the autoxidation of the resulting $[Fe^{II}-(TPA)(OBz)]^+$ complex, since there is no evidence for the formation of $[Fe^{III}_2(O)(TPA)_2(BF)_2]^{2+}$ under our reaction conditions. HPLC analysis of the product benzoic acid after workup of the reactions indicates yields of 95% for **1** and 93% for **2**. Thus, the BF ligand undergoes nearly quantitative oxidative decarboxylation upon exposure to O_2, i.e.

$$[Fe^{II}(L)(PhCOCOO)]^+ + O_2 \rightarrow$$
$$[Fe^{II}(L)(PhCOO)]^+ + CO_2 + [O] \quad (5)$$
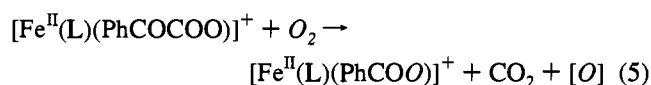
To trap the oxidizing equivalents implied by [O] in eq 5, we have investigated the reactions of complexes **1** and **2** with some potential substrates. The stoichiometric oxidation of 2,4-di-*tert*-butylphenol to 4,4′,6,6′-tetra-*tert*-butyl-2,2′-biphenol occurs with both complexes in CH_3CN at room temperature under an O_2 atmosphere. When the reaction is carried out in the presence of 10 equiv of phenol, 0.75 mol of the corresponding biphenol is formed/mol of complex **1** and 1.0 mol of biphenol/mol of complex **2** (by ^1H NMR) without altering the yields of their product complexes (**5** and **6**, respectively). Control experiments also indicate that both dioxygen and the iron(II) complexes are required to generate the biphenol product. The reactions with phenol are presumably initiated via hydrogen abstraction by an

active oxygen species, giving rise to an intermediate phenoxy radical that readily dimerizes to form the biphenol product (Scheme 1). Thus, most of the oxidizing equivalents resulting from the oxidative decarboxylation of these iron(II)−α-keto-carboxylate complexes can be intercepted in these experiments. Similarly, triphenylphosphine is converted by **1** and **2** in the presence of O_2 to $OPPh_3$ in 61% and 68% yields, respectively.

However, substrates that are more difficult to oxidize afford either small yields of product or no yield at all. For example, thioanisole is oxidized to methyl phenyl sulfoxide in 5−10% yield. Trace amounts of cyclohexanone and dimethyl sulfone can be identified by GC analysis from the oxidation experiments with cyclohexanol and dimethyl sulfoxide, respectively, but cumene and cyclohexane are unreactive. It would thus appear that the oxidizing species generated in the oxidative decarboxylation of **1** and **2** is either less reactive than those associated with the enzymes or decomposes via alternative pathways before it has a chance to react with these substrates.

To ascertain the incorporation of dioxygen in the oxidative decarboxylation reactions, the oxygenation reactions of **1** and **2** were carried out in an $^{18}O_2$ atmosphere with PPh_3 as substrate. The data for the incorporation of ^{18}O into the resulting products are summarized in Table 6. Oxidation of PPh_3 in the presence of $^{18}O_2$ and **1** or **2**, respectively, shows the incorporation of 61% and 85% of ^{18}O label into $OPPh_3$. The less than stoichiometric incorporation of label is not due to solvent exchange with the oxidizing species or $OPPh_3$, since control experiments in $H_2^{18}O$ show no label incorporation into $OPPh_3$ from solvent water, but probably reflects the long reaction times required to effect complete oxidative decarboxylation which may give rise to contamination of $^{18}O_2$ with $^{16}O_2$ from the atmosphere. The larger amount of label incorporation from $^{18}O_2$ found in the reaction of **2**, which occurs on a shorter time scale, is consistent with this explanation.

However, the ^{18}O labeling results for the benzoate derived from the oxidative decarboxylation suggest some complications. The reactions of **1** and **2**, respectively, with $^{18}O_2$ afford benzoate moieties with 40% and 68% of one ^{18}O label incorporated, a level of incorporation that is lower than that found for the corresponding $OPPh_3$ product. These values are not affected by the absence of PPh_3 in the oxygenation reaction. Control experiments were carried out in the presence of trace amounts of $H_2^{18}O$ to determine if solvent water can exchange with the benzoate oxygens. No solvent exchange occurs with the coordinated benzoates in **5** or **6**. On the other hand, solvent water is readily exchanged into **1** and **2**, presumably into the keto oxygen of the BF moiety. When the oxygenation reaction is run in the presence of $H_2^{18}O$, the resulting benzoate can acquire as many as two ^{18}O labels (Table 6). The data for **1**

(32) Ménage, S.; Vincent, J. M.; Lambeaux, C.; Chottard, G.; Grand, A.; Fontecave, M. *Inorg. Chem.* **1993**, *32*, 4766−4773.

(33) Kojima, T.; Leising, R. A.; Yan, S.; Que, L., Jr. *J. Am. Chem. Soc.* **1993**, *115*, 11328−11335.

(34) Hazell, A.; Jensen, K. B.; McKenzie, C. J.; Toftlund, H. *Inorg. Chem.* **1994**, *33*, 3127−3134.

(35) Latos-Grazynski, L.; Cheng, R.-J.; La Mar, G. N.; Balch, A. L. *J. Am. Chem. Soc.* **1982**, *104*, 5992−6000.

(36) Tolman, W. B.; Liu, S.; Bentsen, J. G.; Lippard, S. J. *J. Am. Chem. Soc.* **1991**, *113*, 152−164.

α-*Keto Acid-Dependent Non-heme Iron Enzymes*

J. Am. Chem. Soc., Vol. 117, No. 14, 1995 4009

Table 6. Results from Oxygen-18 Labeling Experiments

	no. of ^{18}O atoms in product	^{18}O$_2$[a]	H$_2$^{18}O[b]
I. Oxidation of [Fe^{II}(6TLA)(BF)](ClO$_4$) (1)			
[Fe^{II}(6TLA)(OBz)]$^+$ (5) (m/z 509)	0	54	25
(derived from oxidation of 1)	1	46	52
	2	c	23
isolated HOBz (m/z 122)	0	60	31
	1	40	49
	2	c	20
OPPh$_3$ (m/z 278)	0	39	96
	1	61	4
[Fe^{II}(6TLA)(OBz)]$^+$ (5)[d] (m/z 509)	0		100
	1		c
[Fe^{II}(6TLA)(BF)]$^+$ (1)[e] (m/z 537)	0		25
	1		75
II. Oxidation of [Fe^{II}(TPA)(BF)](ClO$_4$) (2)			
[Fe^{III}$_2$O(TPA)$_2$(OBz)$_2$](ClO$_4$)$^+$ (6) (m/z 1049)	0	25	7
(derived from oxidation of 2)	1	37	13
	2	28	22
	3	10	24
	4	c	23
	5	c	11
isolated HOBz (m/z 122)	0	32	27
	1	68	43
	2	c	30
OPPh$_3$ (m/z 278)	0	15	100
	1	85	c
[Fe^{III}$_2$O(TPA)$_2$(OBz)$_2$](ClO$_4$)$^+$ (6)[d] (m/z 1049)	0		93
	1		7
[Fe^{II}(TPA)(BF)]$^+$ (2)[e] (m/z 495)	0		17
	1		83

[a] Experiments carried out in ^{18}O$_2$; isotopic distribution values were calculated on the basis of comparisons of the mass spectra of samples from ^{18}O-labeling and from control ^{16}O experiments. [b] Parallel experiments carried out in an ^{16}O$_2$ atmosphere with the addition of trace amounts of H$_2$^{18}O. [c] Not observed. [d] Oxygenation reactions of independently prepared authentic complexes using the same conditions as for complexes 1 and 2. [e] These experiments were carried out in an anaerobic glovebox with the use of deoxygenated CH$_3$CN.
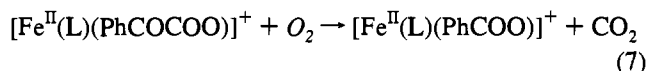
can be analyzed in the following manner. Exchange of H$_2$^{18}O into 1 affords a complex that is 75% singly labeled on the BF oxygen. If no further label is incorporated from solvent during oxygenation, the resulting benzoate should contain an ^{18}O label in 75% of the molecules. However, oxygenation in the presence of H$_2$^{18}O affords benzoate that is 49% singly labeled and 20% doubly labeled. On the basis of the labeling results before and after exposure to O$_2$, 69% (49% + 20%) of the benzoate molecules acquired one label as a result of solvent exchange into the keto oxygen, while 20% of the benzoate gained a second label during the oxidation. This 0.2 atom equivalent of ^{18}O label gained from H$_2$^{18}O matches the 0.2 atom equivalent difference (61% − 40%) between the OPPh$_3$ and benzoate values in the ^{18}O$_2$ experiments. A similar analysis of the data for 2 corroborates the conclusion that solvent water can exchange with a species generated during the oxidative decarboxylation of 1 and 2.

Our interpretation of the labeling results takes into account the fact that only 60−70% of the oxidizing equivalents implied in the oxidative decarboxylation can be trapped by PPh$_3$. We suggest that there are two pathways for the oxidative decarboxylation of 1 and 2, an oxygenation pathway that oxidizes substrate to product and incorporates the elements of O$_2$ into the products (eq 6) and an uncoupled autoxidation pathway that does not involve PPh$_3$ oxidation nor O$_2$ incorporation into the product benzoate (eq 7), i.e.

In the oxygenation pathway, which occurs 60−70% of the time

oxygenation pathway

$$[Fe^{II}(L)(PhCOCOO)]^+ + O_2 + PPh_3 \rightarrow$$
$$[Fe^{II}(L)(PhCOO)]^+ + CO_2 + OPPh_3 \quad (6)$$

uncoupled autoxidation pathway

$$[Fe^{II}(L)(PhCOCOO)]^+ + O_2 \rightarrow [Fe^{II}(L)(PhCOO)]^+ + CO_2 \quad (7)$$
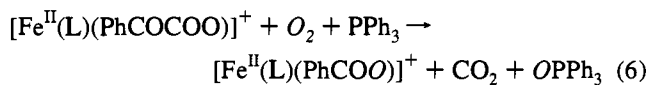
as indicated by the amount of OPPh$_3$ formed, label incorporation is stoichiometric for benzoate and OPPh$_3$. For 1, the 0.61 equiv of OPPh$_3$ formed which has 61% ^{18}O label incorporated should afford 0.61 equiv of 5 with 61% ^{18}O label. The remaining 0.34 (0.95−0.61) equiv of 5 would be produced by the autoxidation pathway and have no ^{18}O label incorporated. Thus, while the ^{18}OPPh$_3$ produced by eq 6 is undiluted, the ^{18}O-labeled 5 produced by eq 6 is diluted by the unlabeled 5 produced by eq 7 to afford a label incorporation of 39% (61% × 0.61/0.95), which is close to what is observed (40%). Analysis of the labeling results for 2 predicts a label incorporation of 62% (85% × 0.68/0.93) into the benzoate, compared to an observed value of 68%.

Kinetics and Mechanistic Implications. The oxidative decarboxylation of a series of [Fe^{II}(6TLA)(X-BF)](ClO$_4$) complexes by dioxygen in acetonitrile can be followed spectrophotometrically. The lack of a visible chromophore for 2 in CH$_3$CN precluded a parallel kinetic study of corresponding TPA complexes. Figure 7 shows the gradual disappearance of the visible features of complex 1 in CH$_3$CN upon exposure to dioxygen at 30 °C. The kinetics were studied under pseudo-first-order conditions with the oxidant (O$_2$) in excess at 30.0 ± 0.1 °C. First-order traces over at least five half-lives were obtained for the decay of the visible absorption peaks, corresponding to the MLCT bands of the starting complex (see Table 4). The following rate law was obtained: rate = k_{obs}[Fe^{II}], where k_{obs} = k[O$_2$]. Table 4 lists values of k_{obs} for all [Fe^{II}-(6TLA)(X-BF)](ClO$_4$) complexes. The nature of the phenyl substituent drastically influences the rate of this reaction for the series of substituted BF complexes, with reaction periods varying from 7 h to 4 days at 30.0 °C. The reaction rate increases in the presence of electron-withdrawing substituents. A good correlation (R^2 = 0.96) is obtained in the Hammett plot of the relative rates vs σ values[37] (Figure 8), and the correlation is poorer if σ^+ values are used. The Hammett plot has a positive slope (ρ = +1.07), indicating a *nucleophilic* mechanism; i.e., withdrawal of electron density at the bound benzoylformate increases its susceptibility for attack by dioxygen species at the carbonyl carbon of BF and facilitates the decarboxylation reaction.

A reaction mechanism proposed for the oxygenation of 1 and 2 is sketched in Figure 9. The general concept of this reaction scheme parallels the mechanisms proposed by Hanauske-Abel and Günzler[2] and by Hamilton.[38] As implicated by the kinetic studies of [Fe^{II}(6TLA)(X-BF)]$^+$ complexes, the first step of the reaction of [Fe^{II}(L)(BF)]$^+$ with dioxygen is the disruption of the π conjugation formed by the chelated, planar benzoylformate to give a five-coordinate iron(II) species (step a). Complex 2 with its monodentate BF ligand (Figure 2), on the other hand, may already be poised for step b. O$_2$ attack at the Fe(II) center

(37) Exner, O. In *Correlation Analysis in Chemistry*; Chapman, N. B., Shorter, J., Eds.; Plenum Press: New York, 1978; pp 439−540.

(38) Hamilton, G. A. In *Progress in Bioorganic Chemistry*; Kezdy, F. J., Kaiser, E. T., Eds.; 1971; Vol. 1, pp 83−157.
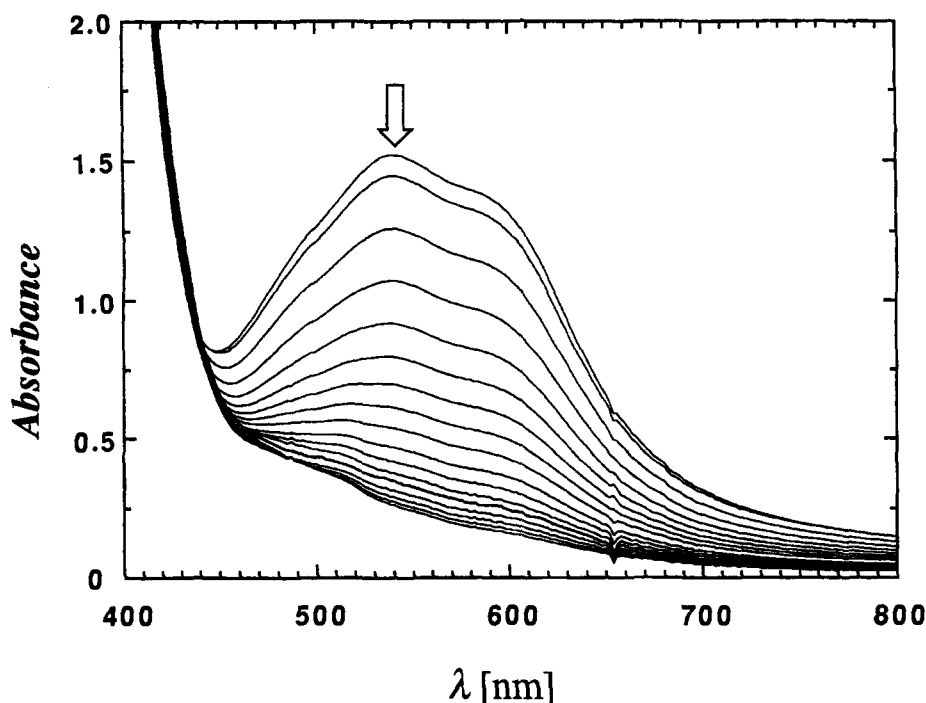
Figure 7. Time-dependent changes of visible absorption features of **1** in CH_3CN at 30.0 °C under an O_2 atmosphere. The time interval between traces is 2.5 h.
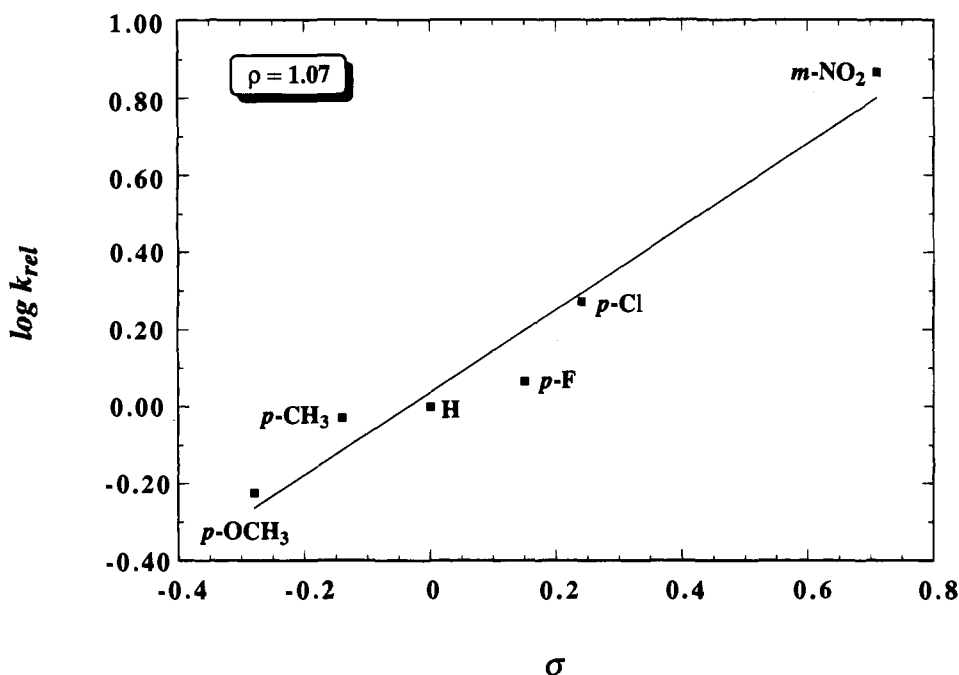
Figure 8. Hammett correlation plot for the rates of oxidative decarboxylation of a series of $[Fe^{II}(6TLA)(X-BF)](ClO_4)$ complexes in CH_3CN at 30.0 °C ($R^2 = 0.96$).

then forms an iron(III)−superoxide species (step b), followed by nucleophilic attack of this superoxide species at the keto carbon of benzoylformate (step c). Release of CO_2 then forms an iron(II)−peracid complex (step d), and subsequent heterolytic O−O bond cleavage affords an iron(IV)−oxo species which is responsible for C−H bond lysis (step e).

Support for steps b−d derives from the observations by Valentine *et al.* that superoxide is a potent nucleophile capable of effecting facile oxidative cleavage of α-keto acids,[39] and that peracids are likely intermediates resulting from the reaction of

superoxide with carboxylic esters.[40] Support for step e has been reported for two synthetic systems: (1) $[Fe^{II}(H_2Hbab)(N-MeIm)]_2$ quantitatively converts phenylperacetic acid to phenylacetic acid, demonstrating heterolytic cleavage of the percarboxylic O−O bond,[41] and (2) $[HB(3,5-iPr_2pz)_3]Fe^{III}(OAr)_2$ reacts with mCPBA to afford an (acylperoxo)(phenoxo)iron(III) species at −78 °C in Et_2O, which upon warming to room temperature quantitatively hydroxylates the bound phenolate to catechol.[42]

(39) San Filippo, J., Jr.; Chern, C.; Valentine, J. S. *J. Org. Chem.* **1976**, *41*, 1077−1078.

(40) San Filippo, J., Jr.; Romano, L. J.; Chern, C.; Valentine, J. S. *J. Org. Chem.* **1976**, *41*, 586−588.

(41) Stassinopoulos, A.; Caradonna, J. P. *J. Am. Chem. Soc.* **1990**, *112*, 7071−7073.
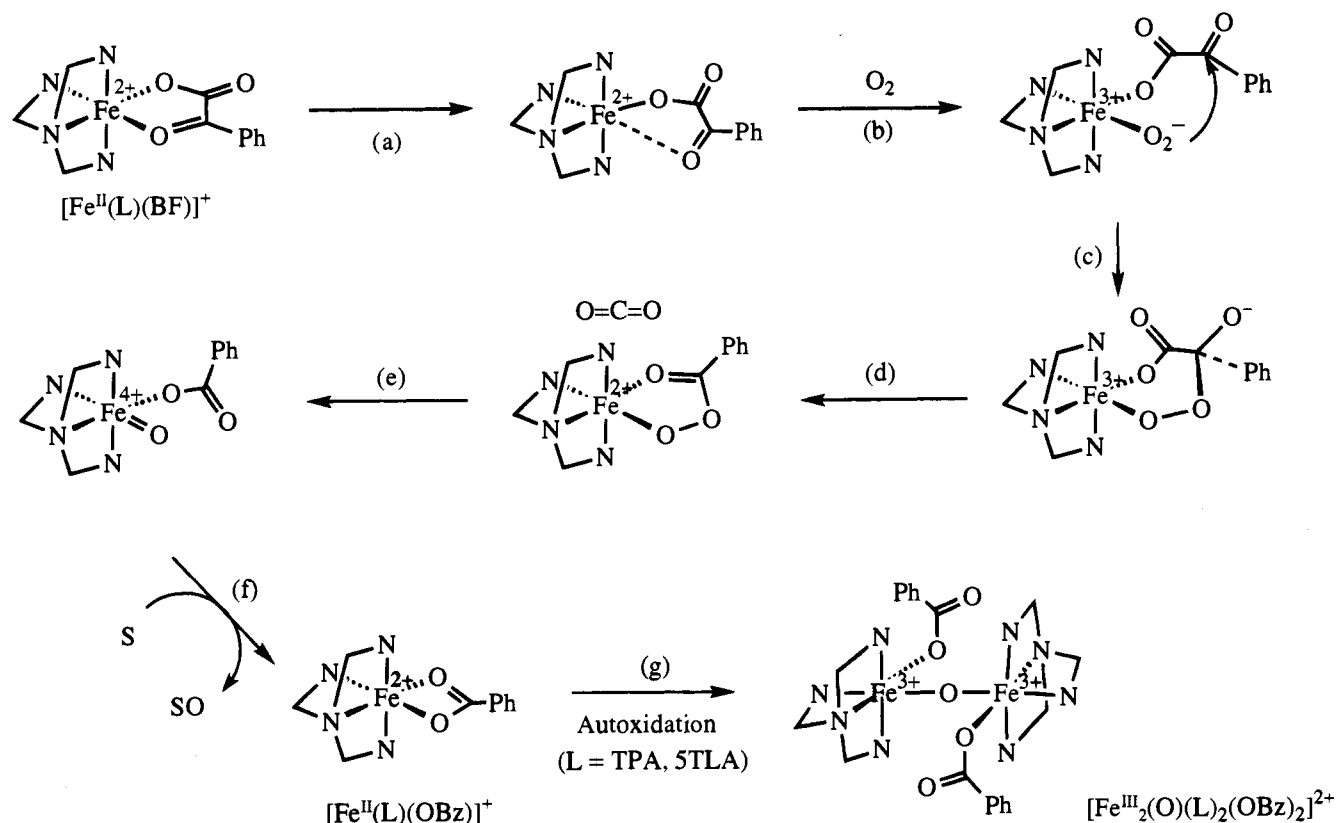
Figure 9. Proposed mechanism for the oxygenation of **1** and **2**.

As illustrated in the reactivity studies, the oxidizing equivalent generated from the oxidative decarboxylation of benzoylformate can be trapped by the oxidation of 2,4-di-*tert*-butylphenol to the corresponding biphenol or triphenylphosphine to triphenylphosphine oxide. The resulting [Fe^{II}(L)(OBz)]$^+$ is the final product when L is the 6TLA ligand (step f). However, when L is TPA or 5TLA, the corresponding iron(II) products, with lower redox potentials than that of the 6TLA complex, undergo further autoxidation reaction to give a (μ-oxo)diiron(III) complex (step g).[23]

Complexes **1** and **2** are proposed to share the same oxygenation mechanism (Figure 9), but the oxidation of **2** is more facile than that of **1**. We propose that the rate difference between the two compounds derives from the steric interactions among the α-methyl groups of the 6TLA ligand, which shift the redox potential of **1** to a more positive value than that of **2**. The higher redox potential of **1** favors the iron(II) state and thus increases the energy barrier of **1** to form an iron(III)—superoxide species upon exposure to O$_2$ in what is likely to be the rate-determining step of the biomimetic reaction.

Relevance to the Biological Systems

In our synthetic models, we have utilized pyridine-based tripodal ligands 6TLA and TPA as a starting point and find that iron(II)—α-ketocarboxylate complexes of both 6TLA and TPA react with O$_2$ to afford oxidative decarboxylation of the iron-bound α-keto acid. Furthermore, we have found in another study that the introduction of one phenolate into the iron coordination sphere accelerates the oxidative decarboxylation reaction by 3—4 orders of magnitude relative to **1** and **2**.[43] The fact that these complexes react with O$_2$ at significantly different

rates demonstrates that the ligand environment plays an important role in this reaction.

There is at present a lack of detailed information about the coordination environment of the iron center in the α-keto acid-dependent iron enzymes. Histidine residues are found in conserved positions in sequence comparisons of prolyl and lysyl hydroxylases from various sources and are modified by diethyl pyrocarbonate to inactivate these enzymes.[44] Tyrosine and histidine residues are also found at conserved positions in a comparison of seven HPP dioxygenases from various mammalian and pseudomonad sources.[45,46] Indeed, resonance Raman studies of the *Pseudomonas* HPP dioxygenase have shown the presence of one *tyrosine* coordinated to the high-spin iron(III) form of the enzyme.[47,48] Thus, the iron(II) environment of these enzymes is likely to have a mixed oxygen/nitrogen coordination sphere like those found for protocatechuate 3,4-dioxygenase (2Tyr/2His),[49] superoxide dismutase (3His/1Asp),[50] and soybean lipoxygenase (3His/1COO⁻).[51,52]

The reaction sequence for α-keto acid-dependent enzymes consists of two half-reactions: the oxidative decarboxylation

(42) Kitajima, N.; Ito, M.; Fukui, H.; Moro-oka, Y. *J. Am. Chem. Soc.* **1993**, *115*, 9335—9336.

(43) Chiou, Y.-M.; Que, L., Jr. *Angew. Chem., Int. Ed. Engl.* **1994**, *33*, 1886—1888.

(44) Myllylä, R.; Günzler, V.; Kivirikko, K. I.; Kaska, D. D. *Biochem. J.* **1992**, *286*, 923—927.

(45) Rüetschi, U.; Odelhög, B.; Lindstedt, S.; Barros-Söderling, J.; Persson, B.; Jörnvall, H. *Eur. J. Biochem.* **1992**, *205*, 459—466.

(46) Rüetschi, U.; Déllsen, A.; Sahlin, P.; Stenman, G.; Rymo, L.; Lindstedt, S. *Eur. J. Biochem.* **1993**, *213*, 1081—1089.

(47) Bradley, F. C.; Lindstedt, S.; Lipscomb, J. D.; Que, L., Jr.; Roe, A. L.; Rundgren, M. *J. Biol. Chem.* **1986**, *261*, 11693—11696.

(48) Lindstedt, S.; Rundgren, M. *J. Biol. Chem.* **1982**, *257*, 11922—11931.

(49) Ohlendorf, D. H.; Lipscomb, J. D.; Weber, P. C. *Nature (London)* **1988**, *336*, 403—405.

(50) Stoddard, B. L.; Howell, P. L.; Ringe, D.; Petsko, G. A. *Biochemistry* **1990**, *29*, 8885—8893.
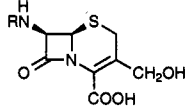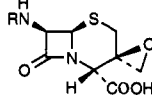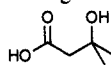
(51) Boyington, J. C.; Gaffney, B. J.; Amzel, L. M. *Science* **1993**, *260*, 1482—1486.

(52) Minor, W.; Steczko, J.; Bolin, J. T. Otwinowski, Z.; Axelrod, B. *Biochemistry* **1993**, *32*, 6320—6323.

Table 7. Presence of Oxygen-18 from Oxygenation Reactions Catalyzed by α-Keto Acid-Dependent Enzymes

enzyme	SO	[$^{18}O_2$] (%)		[$H_2{}^{18}O$] (%)		ref
		RCOO$^-$	SO	RCOO$^-$	SO	
prolyl hydroxylase	hydroxyproline	—	87	—	—	69
lysyl hydroxylase	hydroxylysine	—	6.5	—	—	69
γ-butyrobetaine hydroxylase	D-carnitine	75	—	—	—	67
thymine hydroxylase	5-(hydroxymethyl)uracil	95	91	—	—	68
	5-(1,2-dihydroxyethyl)uracil		97			65
	5-(methylsulfinyl)uracil		97			65
DAOC/DAC synthase		>90^a	50	—	40	63, 70
		—	94	—	17	63, 70
HPP dioxygenase	homogentisate	>95	30	>97	70	71
α-ketoisocaproate oxygenase		>92	15	>94	60	72

^{a} Determined by ^{13}C NMR.

of α-KG concomitant with generation of an oxidizing species and the subsequent functionalization of substrate via a hydrogen-abstraction—recombination step.[2,53] Consistent with this scheme is the uncoupling of the oxidative decarboxylation of α-KG from the alkane functionalization step when substrate analogues are used as observed for prolyl 4-hydroxylase,[54–57] lysyl hydroxylase,[58] thymine 7-hydroxylase,[59] and γ-butyrobetaine hydroxylase.[60,61] The uncoupled decarboxylation reactions proceed at only a fraction of the rate of the whole reaction but nevertheless demonstrate that oxygen activation can proceed in the absence of substrates.

Our model studies have shown that the coordination of an α-keto acid to an iron(II) center facilitates its oxidative decarboxylation. The decarboxylation of BF can occur via a mechanism that is coupled with substrate oxidation (eq 6), which is initiated by nucleophilic attack of an incipient superoxide moiety on the α-keto acid. Alternatively, the decarboxylation of BF can occur via an uncoupled pathway that does not lead to substrate oxidation (eq 7), which parallels observations on the enzymes when poor substrates are used.

The oxidative decarboxylation of α-KG affords an oxidizing species capable of oxo transfer and hydrogen abstraction. This species has been proposed to be an Fe(IV)=O species derived from heterolytic cleavage of the Fe(II)—peroxo intermediate. Support for this notion has come from studies by Pascal *et al.* on HPP dioxygenase,[62] Baldwin et al. on DAOC/DAC synthase,[63] and Thornburg *et al.* on thymine hydroxylase,[64–66]

showing oxo transfer chemistry when appropriate alternate substrates are used and the facile incorporation of solvent water into the products of some enzymes. Table 7 summarizes some of the results from ^{18}O-labeling experiments.[63,64,67–72] Incorporation of labels from $^{18}O_2$ into the carboxylate derived from the oxidation of the α-ketocarboxylate group is nearly quantitative in all cases except one, showing that there is little exchange with this functional group. On the other hand, products derived from the oxygenation of substrate show as little as 6.5% label incorporation to nearly quantitative incorporation. In several cases, solvent water can clearly be incorporated into the oxygenated products. These data are consistent with the participation of an iron—oxo or iron—hydroxy species that can exchange with solvent, given solvent access to the active site. These labeling results on enzymatic reactions differ from those observed for the biomimetic system in that the latter exhibits some tendency for the carboxylate product to incorporate oxygen from solvent. However, for a proper comparison, detailed labeling experiments need to be carried out with the enzymes under conditions that favor uncoupled oxidative decarboxylation of the α-keto acid.

In conclusion, we have synthesized and characterized the first iron(II)—α-ketocarboxylate complexes which provide key chemical precedents for the chemistry carried out by α-keto acid-dependent enzymes. Although the oxidative decarboxylation rates found for the synthetic complexes are orders of magnitude slower than those observed for the enzymes, these complexes nevertheless serve as a starting point for understanding the active

(53) Majamaa, K.; Hanauske-Abel, H. M.; Günzler, V.; Kivirikko, K. I. *Eur. J. Biochem.* **1984**, *138*, 239–245.

(54) Myllylä, R.; Majamaa, K.; Günzler, V.; Hanauske-Abel, H. M.; Kivirikko, K. I. *J. Biol. Chem.* **1984**, *259*, 5403–5405.

(55) Rao, N. V.; Adams, E. *J. Biol. Chem.* **1978**, *253*, 6327–6330.

(56) Counts, D. F.; Cardinale, G. J.; Udenfriend, S. *Proc. Natl. Acad. Sci. U.S.A.* **1978**, *75*, 2145–2149.

(57) Tuderman, L.; Myllylä, R.; Kivirikko, K. I. *Eur. J. Biochem.* **1977**, *80*, 341–348.

(58) Puistola, U.; Turpeenniemi-Hujanen, T. M.; Myllylä, R.; Kivirikko, K. I. *Biochim. Biophys. Acta* **1980**, *611*, 40–50.

(59) Holme, E.; Lindstedt, G.; Lindstedt, S. *Acta Chem. Scand., Ser. B* **1979**, *B33*, 621–622.

(60) Holme, E.; Lindstedt, S.; Nordin, I. *Biosci. Rep.* **1984**, *4*, 433–440.

(61) Holme, E.; Lindstedt, S.; Nordin, I. *Biochem. Biophys. Res. Commun.* **1982**, *107*, 518–524.

(62) Pascal, R. A., Jr.; Oliver, M. A.; Chen, Y.-C. J. *Biochemistry* **1985**, *24*, 3158–3165.

(63) Baldwin, J. E.; Adlington, R. M.; Crouch, N. P.; Pereira, I. A. C.; Aplin, R. T.; Robinson, C. *J. Chem. Soc., Chem. Commun.* **1993**, 105–108.

(64) Thornburg, L. D.; Stubbe, J. *J. Am. Chem. Soc.* **1989**, *111*, 7632–7633.

(65) Thornburg, L. D.; Lai, M.-T.; Wishnok, J. S.; Stubbe, J. *Biochemistry* **1993**, *32*, 14023–14033.

(66) Thornburg, L. D.; Stubbe, J. *Biochemistry* **1993**, *32*, 14034–14042.

(67) Lindblad, B.; Lindstedt, G.; Tofft, M.; Lindstedt, S. *J. Am. Chem. Soc.* **1969**, *91*, 4604–4606.

(68) Holme, E.; Lindstedt, G.; Lindstedt, S.; Tofft, M. *J. Biol. Chem.* **1971**, *246*, 3314–3319.

(69) Kikuchi, Y.; Susuki, Y.; Tamiya, N. *Biochem. J.* **1983**, *213*, 507–512.

(70) Baldwin, J. E.; Adlington, R. M.; Schofield, C. J.; Sobey, W. J.; Wood, M. E. *J. Chem. Soc., Chem. Commun.* **1989**, 1012–1015.

(71) Lindblad, B.; Lindstedt, G.; Lindstedt, S. *J. Am. Chem. Soc.* **1970**, *92*, 7446–7449.

(72) Sabourin, P. J.; Bieber, L. L. *J. Biol. Chem.* **1982**, *257*, 7468–7471.

α-*Keto Acid-Dependent Non-heme Iron Enzymes*

J. Am. Chem. Soc., Vol. 117, No. 14, 1995 4013

site structure and mechanism of this interesting class of non-heme iron enzymes. Further efforts are ongoing to uncover the possible reaction intermediates during the oxidation process and to investigate the effects of different ligand environments.

Supplementary Material Available: X-ray structural information for [Fe(6TLA)(BF)](ClO$_4$) (**1**) and [Fe(TPA)(BF)-(MeOH)](ClO$_4$)·2MeOH (**2·MeOH**), ORTEP drawings with complete labeling scheme and tables of atomic coordinates, thermal parameters, and intramolecular bond lengths and angles (27 pages). This material is contained in many libraries on microfiche, immediately follows this article in the microfilm version of the journal, can be ordered from the ACS, and can be downloaded from the Internet; see any current masthead page for ordering information and Internet access instructions.

JA943732Y